The Physical Properties and Effective Temperature Scale of O-type Stars as a Function of Metallicity. II. Analysis of 20 More Magellanic Cloud Stars, and Results from the Complete Sample[1,2]

Philip Massey[3]

Lowell Observatory, 1400 W. Mars Hill Road, Flagstaff, AZ 86001; Phil.Massey@lowell.edu

Joachim Puls and A. W. A. Pauldrach

Universitäts-Sternwarte München, Scheinerstrasse 1, 81679, Munich, Germany;

uh101aw@usm.uni-muenchen.de,uh10107@usm.uni-muenchen.de

Fabio Bresolin, Rolf P. Kudritzki, and Theodore Simon

Institute for Astronomy, University of Hawaii, 2680 Woodlawn Drive, Honolulu, HI 96822;

bresolin@ifa.hawaii.edu,kud@ifa.hawaii.edu,tsimon@ifa.hawaii.edu

Received _____; accepted _____

DRAFT September 19, 2004

---

[1]Based on observations made with the NASA/ESA Hubble Space Telescope, obtained at the Space Telescope Telescope Science Institute, which is operated by the Association of Universities for Research in Astronomy (AURA), Inc., under NASA contract NAS 5-26555. These observations are associated with programs 6417, 7739, and 9412.

[2]Based on observations made with the NASA-CNES-CSA *Far Ultraviolet Spectroscopic Explorer,* operated for NASA by John Hopkins University under NASA contract NAS5-32985. These observations are associated with program C002.

[3] Visiting astronomer, Cerro Tololo Inter-American Observatory (CTIO), a division of the National Optical Astronomy Observatory, which is operated by the AURA, Inc., under cooperative agreement with the National Science Foundation.

ABSTRACT

In order to determine the physical properties of the hottest and most luminous stars, and understand how these properties change as a function of metallicity, we have analyzed *HST*/UV and high S/N optical spectra of an additional 20 Magellanic Cloud stars, doubling the sample presented in the first paper in this series. Our analysis uses NLTE line-blanketed models that include spherical extension and the hydrodynamics of the stellar wind. Our study also uses far-UV spectra obtained with *FUSE* and near-UV data obtained with *HST* to provide an independent check on the validity of our derived parameters. The results from the complete sample are used as follows: (1) We present a provisional effective temperature scale for O stars as a function of metallicity. We find that the SMC O3-7 dwarfs are 4000 K hotter than Galactic stars of the same spectral type. The difference is in the sense expected due to the decreased significance of line-blanketing and wind-blanketing at the lower metallicities that characterize the SMC. The temperature difference between the SMC and Milky Way stars decreases with decreasing temperature, becoming negligible by spectral type B0, in accord with the decreased effects of stellar winds at lower temperatures and luminosities. The temperatures of the LMC stars appear to be intermediate between that of the Milky Way and SMC, as expected based on their metallicities. Supergiants show a similar effect, but are roughly 3000-4000 cooler than dwarfs for early O stars, with a negligible difference by B0. The giants appear to have the same effective temperature scale as dwarfs, consistent with there being little difference in the surface gravities. Our scale is hotter than that found by WM-BASIC and CMFGEN modeling of different samples of stars by others, but ours leads to a more coeval placement of stars in the H-R diagram of NGC 346. (2) We find that the modified wind momentum of these stars scale with luminosity

and metallicity in the ways predicted by radiatively-driven wind theory, supporting the use of photospheric analyses of hot luminous stars as a distance indicator for galaxies with resolved massive star populations. (3) A comparison of the spectroscopic masses with those derived from stellar evolutionary theory shows relatively good agreement for stars with effective temperatures below 45000 K; however, stars with higher temperatures all show a significant mass discrepancy, with the spectroscopic masses a factor of 2 or more smaller than the evolutionary masses. This problem may in part be due to unrecognized binaries in our sample, but the result suggests a possible systematic problem with the surface gravities or stellar radii derived from our models. (4) Our sample contains a large number of stars of the earliest O-types, including those of the newly proposed O2 subtype. We provide the first quantitative descriptions of their defining spectral characteristics and investigate whether the new types are a legitimate extension of the effective temperature sequence. We find that the NIII/NIV emission line ratio used to define the new classes does not, by itself, serve as an effective temperature indicator within a given luminosity class: there are O3.5 V stars which are as hot or hotter than O2 V stars. Neither do the luminosity criteria proposed for the O2-3.5 classes result in giants which have lower surface gravities or higher luminosities than do dwarfs, although the supergiants can be distinguished spectroscopically from dwarfs and giants. This problem can readily be attributed to the effects that stellar winds have on the spectral appearance of these stars, and merely mean that the NIII/NIV line ratio has to be analyzed in concert with other spectroscopic diagnostic lines, such as Hα. (5) The two stars with the most discordant radial velocities in our sample happen to be O3 "field stars", i.e., found from the nearest OB associations. This provides the first compelling observational evidence as to the origin of the field O stars in the

Magellanic Clouds; i.e., that these are classic runaway OB stars, ejected from their birth places.

Subject headings: stars: early-type, stars: atmospheres, stars: fundamental parameters, stars: mass loss

1. Introduction

An accurate knowledge of the stellar effective temperature scale provides the means of converting the observed properties of a star into its physical properties. The issue is particularly important—and challenging—for the massive O-type stars, as the bolometric corrections (BCs) are a very steep function of the assumed effective temperature ($T_{\rm eff}$) at the extremely high $T_{\rm eff}$'s that characterize these objects. For these hot stars, a 10% error in $T_{\rm eff}$ results in in an error of 30% in the derived luminosity of a star, compromising any attempt to use stellar evolutionary tracks to determine distances, initial mass functions (IMFs), and ages of clusters (see, for example, Massey 1998; Slesnick et al. 2002). In addition, a 10% uncertainty in $T_{\rm eff}$ results in a factor of 2 or more uncertainty in the Lyman continuum flux, affecting our understanding of the ionization balance of H II regions and the porosity of the interstellar medium in general (see, for example, Oey & Kennicutt 1997, Oey 2004).

At the same time, the determination of the effective temperature scale of O-type stars is complicated by the fact that the stellar atmospheres of these stars are physically complex. The strong spectral features are formed under non-local thermodynamic equilibrium (NLTE) conditions (Auer & Mihalas 1972), while stellar winds provide a significant source of heating of the photosphere through the backscattering of radiation (Hummer 1982; Abbott & Hummer 1985). Modern stellar atmosphere models for O-type stars include NLTE, spherical extension, the hydrodynamics of the the stellar winds, and the effects of line blanketing; see, for example, Pauldrach et al. (2001), Hillier et al. (2003), and Puls et al. (2003) for descriptions of the stellar atmosphere programs WM-BASIC, CMFGEN, and FASTWIND, respectively.

The most recent improvement in these code is a more exact treatment of line blanketing. The results of fitting these improved models to stars have suggested that the previous

effective temperature scale for Galactic O stars may be too hot by as much as $\sim 20\%$ (see, for example, Repolust et al. 2004, Garcia & Bianchi 2004, Bouret et al. 2003, Hillier et al. 2003, Bianchi & Garcia 2002, Crowther et al. 2002, and Martins et al. 2002).

We are engaged in a new determination of the effective temperature scale of O-type stars, with an emphasis on how the conversion from spectral type to $T_{\rm eff}$ depends upon the initial composition of the gas out of which the star was formed; i.e., how do the physical properties of an O7.5 V star differ in the SMC, LMC, Milky Way, and the Andromeda Galaxy, systems which span a range of 10 in metallicity. In a previous paper (Massey et al. 2004, hereafter Paper I) we analyzed the spectra of a sample of 20 SMC and LMC O-type stars using FASTWIND. The same code has recently been used to analyze a sample of Galactic O-type stars (Repolust et al. 2004). Our study suggested that the Magellanic Cloud sample was 3,000-4,000 K hotter than their Galactic counterparts for the early through mid-Os, although the sample size precluded a more definitive statement.

Here we extend these studies to an additional sample of 20 Magellanic Cloud O-type stars, and consider the results from the complete sample of 40 stars. In Sec. 2 we describe the space- and ground-based data of the new sample, along with our reduction procedures. In Sec. 3 we provide the model fits to these spectra, determining physical parameters, and describe the spectrum of each star in turn (Sec. 3.1). Our data includes very high S/N spectra of stars of the earliest types, including the newly proposed "O2" type (Walborn et al. 2002), and in Sec. 4 we provide the first quantitative classification criteria for such stars. Our analysis also allows us to investigate whether the physical properties of such stars are well correlated with the new spectral subtypes (i.e., are O2 V stars necessarily hotter than stars classified as O3 V or O3.5 V?). Our analysis of the complete sample of 40 stars then allows us to compare the physical properties of such stars as a function of metallicity (Sec. 5), including deriving effective temperature scales for the SMC, LMC, and Milky

Way (Sec. 5.1) O stars, comparing the modified Wind Momentum Luminosity relationship (Kudritzki et al. 1995) to that expected from radiatively-driven wind theory (Sec. 5.2), and investigating whether or not the derived spectroscopic masses agree well with the masses obtained from stellar evolutionary models (Sec. 5.3). We summarize our conclusions and lay out the need for future work in Sec. 6.

2. Observations and Reductions

The stars are listed in Table 1. As discussed in Paper I, good photometry provides the key to an accurate value of the absolute visual magnitude M_V, needed in order to constrain the stellar radius. Unless otherwise noted in the table, the photometry comes from the CCD *UBV* measurements by Massey (2002) or Massey et al. (2000), except for the R136 stars, which comes from the WFPC2 photometry of Hunter et al. (1997). Conversion to M_V for the non-R136 stars was done by using the color excesses determined from the spectral types (see Paper I), adopting distance moduli of 18.9 and 18.5 for the SMC and LMC respectively, following Westerlund (1997) and van den Bergh (2000). The M_V values for the R136 stars were derived in a similar manner by Massey & Hunter (1998).

The spectroscopic observations are summarized in Tables 2 and 3. In general, our modeling efforts require data in the UV in order to determine the terminal velocity v_∞ of the stellar wind. These data we have obtained with Space Telescope Imaging Spectrograph (STIS) on *HST* using the FUV-MAMA detector. Data in the blue-optical region is used to constrain both the surface gravity g (from the wings of the Balmer absorption lines) and the effective temperatures $T_{\rm eff}$ (from the He I and He II absorption lines). For all but the R136 stars, high S/N spectroscopy was obtained in this region using the CTIO 4-m telescope and RC spectrograph. Spectra of the R136 stars come from CCD observations with *HST*/STIS. Finally, data at Hα is needed to determine the mass-loss rate $\dot{M}$. For this we relied both

upon ground-based CTIO and/or STIS observations. Full details can be found in Paper I.

In addition, we also obtained data in two other wavelength regions for a few of our stars to provide some independent check on the modeling—how well do the models do in reproducing the spectra in wavelength regions not explicitly used for the modeling? The first of these regions was obtained with *HST*/STIS-CCD in the near-UV (NUV) region in order to observe the He I $\lambda 3187$ and He II $\lambda 3203$ lines. We found relatively good agreement in Paper I for the two stars that were observed in the region. Of more critical interest is the far-ultraviolet (FUV) region. We obtained data in the wavelength range 905Å-1187Å with the *Far Ultraviolet Spectroscopic Explorer (FUSE)* satellite (Moos et al. 2000). This spectral region contains the high excitation O VI $\lambda\lambda 1032, 1038$ doublet, which provides a useful check on the determination of v_∞ (see Figs 5 and 6 of Taresch et al. 1997).

The reduction procedure for both the *HST* and CTIO data are given in Paper I, and are not repeated here other than to note that the CCD spectra (both STIS and CTIO) were reduced with IRAF[1] using the optimal extraction algorithms. For the *HST*/STIS data, this led to a substantial improvement in S/N over that delivered by the pipeline (see Fig. 1 of Paper 1). For the STIS UV observations we used the standard pipeline reductions, as we found that reanalysis of these data made no improvement to that of the pipeline.

The *FUSE* data were reprocessed....TED'S PARAGRAPH GOES HERE.

FUSE data are obtained in 8 channels (LiF1a, LiF1b, LiF2a, LiF2b, SiC1a, SiC1b, SiC2a, and SiC2b). For four of the stars, the agreement between the channels was good in the regions of overlap, and we averaged the data to produce a higher S/N spectrum, binned

[1]IRAF is distributed by the National Optical Astronomy Observatories, which are operated by the Association of Universities for Research in Astronomy, Inc., under cooperative agreement with the National Science Foundation.

at 0.1 Å. For one of the stars, AV 177, the agreement between the 8 channels of *FUSE* was poor, with only two of the channels (LiF1a and LiF1b) showing the expected flux levels and a normal spectrum. The observation was repeated at our request, but the new data suffered from an even worse problem involving data drop out, and we obtained useful data only from Li1a and LiF2b. We combined these four observations for our treatment of AV 177.

3. Analysis

Following the procedures of Paper I, we first determined the star's terminal velocity v_∞ from radiative transfer fits of the P Cygni profile of the C IV λ1550 doublet, and (where possible) Si IV λ1400 and N V λ1240, although the Si IV line is usually too weak, and the N V line is often contaminated by strong interstellar Lyα absorption. The fitting is done based upon the SEI method (see Lamers et al. 1987, Haser 1995, and Haser et al. 1995). We list the resultant values in Table 4. We estimate our uncertainty in this procedure as 50-100 km s^{-1}, with larger uncertainties (up to 200 km s^{-1}) indicated by ":". Two stars had even less certain measurements, and we estimate the uncertainties as 300 km s^{-1} [FABIO—do you agree?].

In running the FASTWIND models, we adopted these values of v_∞ and began with the assumption that β (a measure of the steepness of the velocity law) has a value of 0.8 following Puls et al. (1996). In addition, we began by adopting a He/H number ratio of 0.1, and adjusted it if needed. The absolute visual magnitudes M_V were drawn from Table 1, and constrained the stellar radius of each model. We assumed a metallicity $Z/Z_\odot$ of 0.2 for the SMC stars and 0.5 LMC stars, as argued in Paper I. Following Repolust et al. (2004), we adopted a micro-turbulence velocity of 10 km s^{-1} for the models with effective temperatures of 36,000 K and below, and 0 km s^{-1} for the hotter models.

For each star, we ran a series of grids, allowing then the values for $T_{\rm eff}$, $\log g$, and $\dot{M}$ to vary, until we had satisfactory fits (as judged by eye) between the synthetic and observed spectra. In a number of cases, a good fit to the strengths of the He I and He II lines necessitated a slight increase in the He/H ratio, as described below.

As discussed both by Repolust et al. (2004) and in Paper I, FASTWIND does not produce a strong enough He I λ4471 line for giants and supergiants of spectral type O6 and later. Fortunately the He I λ4387 line can be used for these spectral types, with simultaneous good fits to this line and the He II absorption. Subsequent investigation by co-author J.P. has demonstrated that the same problem is encountered with CMFGEN, consistent with our statement in Paper I that this is an example of a long-standing problem with stellar atmosphere codes (see Voels et al. 1989). This so-called "dilution effect" is yet to be understood.[2]

Below we discuss the individual stars in our sample. In determining the spectral types, we first consider the visual impression of the spectra, following the premises of Walborn & Fitzpatrick (1990). We then measured the equivalent widths of He I λ4471 and He II λ4542, the principle classification lines, and determined $\log W' = \log W(4471) - \log W(4542)$, and compared that to that used to differentiate the spectral subtypes by Conti & Alschuler (1971). In practice, there was no disagreement between these two methods. For the earliest type stars, we also make reference to the new classification criteria proposed by Walborn et al. (2003, 2004), based upon the strengths of the N IV λ4058 and N III $\lambda\lambda 4534, 42$ emission

[2]These tests also reveal an *additional* problem with the He I singlets in CMFGEN. This has generally led to the cooler temperatures found with CMFGEN vs. FASTWIND, and accounts for the systematics suggested in Fig. 26 in Paper I; work by Hillier is in progress to correct the CMFGEN problem. [JO–We have to think how we can safely say/reference all this....]

lines and the N V $\lambda 4603, 19$ absorption lines. Walborn et al. (2003) used this to attempt to break the degeneracy of the O3 spectral class and introduced types O2 (N IV>>N III), and redefined O3 as "weak He I with N IV>N III". In Sec. 4 we attempt to provide a slightly more quantitative description. One needs to keep in mind, however, that there is yet to be a demonstration that stars classified as "O2" are necessarily hotter than stars classified as "O3", although this is clearly the implication of the scheme; we also examine this in Sec 4. Furthermore, as emphasized in Paper I, there is no *a priori* basis for assuming that the "Of" characteristics (He II $\lambda 4686$ and N III $\lambda\lambda 4634, 42$ emission) will scale with luminosity in the same way in the SMC than in the Milky Way, given the factor of 4 difference in metallicity between these two systems, and the corresponding differences in stellar winds. N III $\lambda\lambda 4634, 42$ emission is a complex NLTE effect and its size mainly due to effective temperature (Mihalas & Hummer 1973, Taresch et al. 1997), while He II $\lambda 4686$ will depend upon the stellar wind properties, such as density and temperature. Accordingly, we will note any discrepancies between these traditional luminosity indicators and the actual M_V of the stars.

The model fits give us a measure of the *effective* surface gravity $g_{\rm eff}$ which will be the combination of the *true* surface gravity $g_{\rm true}$ offset by centrifugal acceleration due to the rotation of the star. This correction is estimated (in a statistical sense) as simply the square of the projected rotational velocity divided by the stellar radius:

$$g_{\rm true} = g_{\rm eff} + \frac{(v \sin i)^2}{6.96 R} \tag{1}$$

(Repolust et al. 2004), where the numerical factor allows the use of the usual units; i.e., km s^{-1} for $v \sin i$ and solar units for R. We have a good estimate of $v \sin i$ from comparing the model lines with the objected spectra, except that our spectral resolution results in a minimum "rotational" velocity of (generally) 110 km s^{-1}. However, for these stars with minimal rotational velocities the centrifugal correction is tiny (0.01 in $\log g$),

and insignificant compared to the typical fitting uncertainty of 0.1 in $\log g$ (Paper I and Sec. 5). However, for the fast-rotators in our sample the correction can be marginally significant, amounting to 0.05 dex in several cases, and 0.13 dex in one case (AV 296, from Paper I). The spectroscopic masses should be determined from the true surface gravities; i.e., $M_{\rm spect} = (g_{\rm true}/g_{\odot})R^2$.

The final values for the fits are given in Table 5. If we were only able to determine a lower limit to $T_{\rm eff}$ then values for $\log g$, R, $\dot{M}$, and the derived $M_{\rm spect}$ will be approximately correct, while only a lower limit will be known for the total luminosity. Note that in Paper I the stars with only a lower limit on $T_{\rm eff}$ had their stellar radii incorrectly listed as lower limits as well.

3.1. Comments on Individual Stars

3.1.1. SMC

AV 177.—This star was previously classified as O5 V by Crampton & Greasley (1982). Visually, we would classify the star as an O4 V((f)) (Fig. 1a). This is confirmed by our measurement $\log W' = -0.75$. The strength of He I λ4471 (EW=170mÅ) would preclude it being classified as an O3. The luminosity class "V" based upon the strong He II λ4686 absorption is consistent with the star's absolute visual magnitude, $M_V = -4.8$. There is a trace of emission at N III $\lambda\lambda 4634, 42$ (EW~ -250mÅ) leading to the "((f))" designation; there is no sign of N IV λ4058 emission. We obtained satisfactory fits with a slightly increased He/H number ratio (0.15), as shown in Fig. 1b. The mass-loss rate is low ($< 5 \times 10^{-7} M_{\odot}$ yr^{-1}), and only an upper limit can be established. (A value of $3 \times 10^{-7} M_{\odot}$ yr^{-1} is used in the fitting.) The Hα profile obtained from the ground-based data agrees well with the *HST* data; we use the former, since its S/N is greater.

AV 435.—This star had been previously classified as O4 V by Massey et al. (1995). Here we would call it an O3 V. Although He I λ4471 is weakly present (Fig. 2a), its equivalent width is only 125mÅ. This is comparable to or smaller the strength seen in the original O3 V prototypes HD93128 and HDE 303308 (Simon et al. 1983), as well as the other star used by Walborn (1971a) to define the O3 class, HD 93250 (Kudritzki 1980). Walborn et al. (2002) has proposed revising the early O-type classes based upon the strength of selective emission lines, e.g., N IV λ4058 and N III $\lambda 4334, 42$. Since N IV λ4058 is (weakly) present (EW=-80mÅ), with N III emission weaker (EW> -60mÅ), this would also lead to an O3 V((f*)) classification according to these revised criteria. The ((f*)) simply refers to the fact that N IV λ4058 is in emission and equal or stronger than any N III emission. The absolute visual magnitude $M_V = -5.8$ would be consistent with either the "V" or "III" luminosity class; see Conti (1988). The fits we obtained (Fig. 2b) are a good match to the observed spectrum. Again we found the agreement between the ground-based Hα profile and that obtained with *HST* is good, and show the former in the figure.

AV 440.— Previously the star had been classified as O7 V by Walborn (1983), but it is clear in our spectrum (Fig. 3a) that He I λ4471 is somewhat stronger than He II λ4542, and visually we would call this an O8 V star. We measure $\log W' = +0.12$, in accord with this determination. The absolute magnitude $M_V = -4.9$ is consistent with the "V" luminosity class suggested by the star's He II λ4686 absorption.

In order to find a good fit, we needed to again slightly increase the He/H number ratio from the canonical 0.10 to 0.12. This allowed us to then obtain excellent matches to the He II lines (Fig. 3b). However, the model's He I λ4471 line is much weaker than observed; this effect was discussed extensively by Repolust et al. (2004) and by ourselves in Paper I. It seems to primarily affect stars the middle and late O-type giants and supergiants, but here we see it in a dwarf. We instead rely upon the He I λ4387 line, for which the fit *is* good.

The He I λ4713 line (not shown) also is well matched by the model. No ground-based Hα was obtained, and so we rely upon the *HST* observation for the mass-loss determination. Although we used a value of $1 \times 10^{-7} M_{\odot}$ yr^{-1}, in fact we could only set an upper limit on the mass-loss rate ($\dot{M} < 3 \times 10^{-7} M_{\odot}$ yr^{-1}).

AV 446.—This star was classified as O6.5 V by Garmany et al. (1987). We measure $\log W' = -0.13$, consistent with this classification. The only spectral anomaly is that the line *depth* of He I λ4471 is somewhat greater than that of He II λ4542 in our spectrum (Fig. 4a), even though the He I line has a smaller equivalent width. This implies that the line widths differ. This is usually an indication of a binary (see, for example, Walborn 1973a and the follow-up study by Massey & Conti 1977). However, the absolute magnitude $M_V = -4.7$ is indicative of a single star with luminosity class "V", consistent with the spectral appearance. The good agreement of the model and observed spectra (Fig. 4b) also supports a single-star interpretation. A comparison of the ground-based and *HST* Hα profile shows reasonable agreement, and so we used the higher S/N ground-based data for the fit. Once again we could set only an upper limit on the mass-loss rate.

AV 476.—This star was classified as an O6.5 V by Massey et al. (1995). Our higher S/N spectrum, shown in Fig. 5, would suggest a somewhat earlier type. We measure $\log W = -0.34$, indicative of a spectral type of O5.5. He II λ4686 is comparable in strength to He II λ4542, and there is no sign of N III $\lambda\lambda 4634, 42$ emission. Thus if this were a Galactic star, we would assign a luminosity class of "V". The high absolute visual luminosity of this star $M_V = -6.3$ is more in keeping with the star being a giant. We argued in Paper I that these "f" characteristics should not (and often do not) scale with luminosity the same way in the metal-poor SMC as they do in the Milky Way, as the He II λ4686 emission that is used as luminosity indicator will be weaker (at the same luminosity) in the SMC as the stellar winds are weaker. An alternative explanation could be that this

star is a binary, and the spectrum composite. Our fitting efforts are consistent with the latter interpretation in this case, as the hydrogen and He II lines have a very high radial velocity (270 km s^{-1}) which is not shared by the He I velocities. There is a hint of N IV λ4058 emission in the spectrum (Fig. 5), and we suggest that this star is an O2-3 V plus a somewhat latter O-type. We note in passing that there is significant nebular contamination in the ground-based Hα profile.

3.1.2. The non-R136 LMC Stars

Sk−67°22.—Classically, we would classify this star as O3If*/WN, where the second part of the nomenclature simply denotes that the emission features are comparable to what might be found in a Wolf-Rayet star (see Fig. 6a). Indeed, this star was one of the first to be described with this "intermediate" designation (Walborn 1982). Nevertheless, its spectrum is quite unlike that of a typical Wolf-Rayet star, in that its absorption-line spectra lacks P-Cygni components, and it is much more like an ordinary O-type star than more extreme "intermediate" stars, such as Br 58 discussed below. Nevertheless, the "slash" designation resulted in its being included in the recent compilation of Wolf-Rayet stars in the LMC (Breysacher et al. 1999). Were it to be classified according to the Walborn et al. (2002) criteria, it would have to be considered to be an O2If*, as N IV λ4058 emission is much stronger than the slight NIII $\lambda\lambda 4634, 42$ emission visible on the blue wing of He II λ4686, and there is no hint of He I λ4471 in our spectrum. However, Walborn et al. (2002) explicitly excluded O3If*/WN objects from consideration when discussing the O2 spectral class. Following in these footsteps, should we call this star an O2If*/WN? It seems to us that *all* of the so-called "O3If*/WN" stars might be similarly reclassified as O2 If*. The prototype (and until Paper I, the only member) of the O2 If* class is the star HD 93129A, which has relatively weak He II λ4686. However, as reported by Nelan et al. (2004) has now

split HD 93129A into two components ($\Delta m = 0.5$ mag) separated by 60mas, which might account for the weaker emission. In Sk= 67°22 the NIV λ4058 emission is almost identical in strength to that of R136-020 (discussed in Paper I), while the He II λ 4686 line is nearly twice as strong. Several additional examples will be discussed below, and a comparison of their spectra made in Sec. 4. C IV λ4658 is present (EW=-300mÅ) in emission.

Despite the strong emission, our fitting was straightforward, and good relatively good fits were obtained (Fig. 6b). We had to increase the He/H ratio to 0.3 to obtain He lines of the right strength relative to H. Only a lower limit could be set on $T_{\rm eff}$ since no He I could be detected. However, if the temperature were 45,000 K rather than 42,000 K we would have to significantly increase the He/H ratio even further to maintain a good fit. We note that this star has a large projected rotational velocity ($v \sin i = 200$ km s^{-1}) compared to most of the other stars in our sample, and we offer the speculation that the chemical enrichment implied by He/H$\sim$ 0.3 and the strong emission are both coupled to this. As Maeder & Meynet (2000) demonstrate, high rotational velocities can result in efficient mixing of processed material from the core of a star, and it can also lead to enhanced mass-loss, particularly from the poles.

The radial velocity of this star is quite large, 430 km s^{-1}, and is about 150 km^{-1} greater than the systemic velocity of the LMC (Kim et al. 1998). A similar radial velocity was seen in both of our CTIO spectra (blue and Hα) as well as our *HST* Hα spectrum; otherwise we would be inclined to believe this might be a binary. This star was cited by Massey (1998) as an example of an isolated (field) O3 star. Its high radial velocity suggests that it is a runaway star, ejected from its birth place.

Sk−65°47.—This star was classified as O4 If on the basis of the present spectrum (Fig. 7a) by Massey et al. (2000). Here we concur with this type. He I λ4471 is only weakly present, with an equivalent width $W = 115$mÅ. Given the weakness of He I λ4471, we might

be tempted to reclassify the star as O3, were it not for the for the fact that $\log W' = -0.68$, consistent with the O4 classification. Furthermore, Walborn et al. (2002) suggest that for an O3.5 N III $\lambda 4634, 42$ emission is similar in strength to N IV $\lambda 4058$ emission, while here we find N III > N IV (although the latter is clearly present), also leading us to the O4 subtype. The strengths of the N III $\lambda 4634, 42$ and He II $\lambda 4686$ emission lines lead to the "If" luminosity class. This is consistent with the absolute magnitude $M_V = -6.4$, a value which is typical for an O4 If star (Conti 1988). Good fits to the lines were easily found (Fig. 7b), and the physical parameters are well constrained.

LH58-496.—This star was classified as O3-4 V by Conti et al. (1986) and Garmany et al. (1994). Our higher S/N data (Fig. 8a) suggests a later type, O5 V, consistent with our measurement of $\log W' = -0.52$. The absolute magnitude, $M_V = -5.1$, is in good agreement with our spectral classification of a dwarf. We obtained a good fit (Fig. 8b), except for the Hβ profile which is likely filled in by emission. The Hα data were obtained with *HST* and thus provides a relatively nebular-free profile.

LH81:W28-23.—This star was previously classified as O3 V by Massey et al. (2000) based on the same data as used here. Although He I $\lambda 4471$ is readily identified in our spectrum (Fig. 9a), its presence is due to the high S/N, as we measure an equivalent width of only 80mÅ. We find a value of $\log W' = -1.0$, well below the value -0.6 that separates the O4's from the O5's (Conti 1988). N V $\lambda\lambda 4603, 19$ absorption is clearly present, and N IV $\lambda 4058$ emission (EW -120mÅ) is less than that of N III $\lambda\lambda 4634, 42$ (EW = -500mÅ). Thus under the Walborn et al. (2002) scheme, the star would be classified as "O3.5 V((f+))", with the "((f+))" denoting N III emission with comparable Si IV emission. The strong He II $\lambda 4686$ absorption indicates that the star is a dwarf, consistent with its $M_V = -5.1$ value.

Our modeling of this star was straightforward, although it quickly became clear that

we had to significantly increase the He/H number ratio from its canonical 0.1 value to 0.25 in order to match the observed spectrum. The final fits are shown in Fig. 9(b). The ground-based Hα profile agrees well with that obtained with *HST*; accordingly, the former is shown, as it is considerably less noisy.

LH90:Br58.—This star was included in the catalog of LMC Wolf-Rayet stars by Breysacher (1981), who classify it as a WN5-6, and reclassified by Testor et al. (1993) as WN6-7. The lower Balmer lines are in emission (Hα) or P Cygni (Hγ, Hδ), and He II λ4200 and λ4542 are present primarily in absorption (Fig. 10), leading Massey et al. (2000) to argue that the star is more properly called an O3 If/WN6. The equivalent width of He II λ4686 is -18Å; usually -10 is taken (somewhat arbitrarily) as the dividing line between an Of star with strong emission line and a bona-fide Wolf-Rayet star of the WN sequence. Clearly the emission is considerably greater than in Sk$-67°22$ (Fig. 6a). We note that there is little evidence from a visual examination of the spectrum that there is enhanced helium present at the surface of the star, and a more detailed analysis than what we can perform is needed to argue if nitrogen is enhanced or not.

In any event, the strong emission defeated our efforts to obtain an acceptable fit. We did establish that a steep velocity law ($\beta = 3.0$) and high mass-loss rate ($40 \times 10^{-6} M_{\odot}$ yr^{-1}) gave an excellent fit to the Hα profile, with a temperature of 40,000-42,000 K giving a reasonable match to the He II line strength if a $\log g = 3.5$ was assumed. However, our fit is no where near the quality of that of our other stars, as clearly the treatment of the stellar wind dominates the stellar parameters. If these parameters are even approximately correct, the star is quite luminous ($\mathrm{M_{bol}} = -11.1$) with a radius of $30R_{\odot}$ and hence an inferred spectroscopic mass $> 100M_{\odot}$. An analysis that includes chemical abundances (not possible with FASTWIND) is clearly warranted for this interesting object. We do not include this star in our analysis in Sec. 5.

LH90:ST2-22.—This star was classified as O3 III(f*) by Schild & Testor (1992), and reclassified as O3 V((f)) by Massey et al. (2000) based upon the same spectral data as used here. The spectrum in shown in Fig.11a. He I λ4471 is weakly present (EW of 140mÅ), with $\log W' = -0.85$. Should this star be instead classified as an O4? We find N IV λ4058 emission weaker of N III $\lambda\lambda 4634, 42$ (EW of -200mÅ versus EW=-700mÅ), with the presence of N V $\lambda\lambda 4603, 19$ absorption uncertain. Thus according to the criteria given by Walborn et al. (2002) we would classify this star as an O3.5 were we to rely upon the nitrogen emission lines. As to the luminosity class, the prototype O3.5 III(f*) star Pismis 24-17 (Walborn et al. 2002) clearly has much stronger N V $\lambda\lambda 4603, 19$ absorption (compare Walborn et al. 2002 Fig. 4 with our Fig. 11 a), although the N IV and N III emission appears stronger in LH90:ST2-22 than in the O3.5 V(f+) star HD 93250. The appearance of He II λ4686 suggests a giant (III) luminosity class. The absolute magnitude of LH90:ST2-22 is -6.4, which is more typical of an O3-4 *super*giant (O3-4 I) than a dwarf (Table 3-1 of Conti 1988). We adopt O3.5 III(f+) as the spectral type, where the "+" denotes that Si IV $\lambda\lambda 4089, 4116$ is in emission, a somewhat redundant reminder given that all stars so classified have this feature (see Walborn et al. 2002).

The fitting of this star was straightforward. The widths of the Balmer line wings necessitated a value $\log g = 3.7$. The fits are shown in Fig. 11b. A slightly elevated He/H number ratio (0.2) was needed in order to get the helium lines as strong as what was observed.

BI 237.—This star was classified as an O3 V by Massey et al. (1995) using older, poorer S/N data than what we have obtained for the present study. The spectrum is shown in Fig. 12a. We see that this star is somewhat earlier than that of LH90:ST2-22 (Fig. 11a) discussed above, with He I λ4471 nearly absent. We do detect *some* He I λ4471, but at a very weak level ($\sim$ 20mÅ), a detection possible only with our extremely high (500)

S/N spectrum. With the EW of He II λ4542 $\sim$ 750mÅ we conclude $\log W' \sim -1.6$! The nitrogen emission line criteria proposed by Walborn et al. (2002) would make this either an O2 V((f*)) ["NIV >> NIII, no He I"] or an O3 V((f*)) ["NIV > or $\approx$ N III; very weak He I"], given that N IV λ4058 emission (EW=-165mÅ) is stronger than the N III $\lambda\lambda 4634, 42$ emission (EW=-90mÅ).

Whether one should call the star an O2 or an O3 is of course dependent upon the interpretation of the non-quantitative criteria enumerated by Walborn et al. (2002). However, the presence of C IV λ4658 *emission*, with an EW=-140mÅ, (also seen in BI 253, discussed below) is taken by Walborn et al. (2002) as an extreme hot O2 spectrum. We therefore call the star an O2 V((f*)), despite the (very) weak presence of He I λ4471. The absolute magnitude ($M_V = -5.4$) is consistent with the dwarf designation suggested by the strong He II λ4686 absorption feature (Fig. 12a).

Despite the extreme spectral type, the fitting was very straightforward, with the only complication that the He II λ4200 profile was corrupted. The fit is shown in Fig. 12b. The physical parameters are extremely well constrained thanks to the very weak presence of He I λ4471. The *HST* Hα profile agrees well with the higher S/N ground-based data, and thus we used the latter.

This star is one of the "field" early-type stars identified by Massey et al. (1995), located well outside the nearest known OB association (LH 88). We do note that the radial velocity of this star is quite high ($\sim$ 400 km s^{-1}), compared to the systemic LMC velocity of 279 km s^{-1}). Thus this field O2 star would also qualify as an OB runaway. In concert with the similar results for the field O3 star Sk$-67°22$, we believe this provides an explanation for the long-standing mystery of such early-type field stars (Massey et al. 1995; Massey 1998).

BI 253.—This star has many similarities to BI 237. It too was classified as O3 V by

Massey et al. (1995), but was part of the basis for Walborn et al. (2002)'s extension of the spectral sequence to O2. Based upon the spectrum we obtained as part of the present study, Walborn et al. (2002) propose BI 253 as the prototype for the newly defined O2 V class. It is interesting to compare its spectrum (Fig. 13a) with that of BI 237 (Fig. 12a), which we argue above is also a member of the O2 V class. The nitrogen spectrum would suggest that BI 253 is somewhat hotter, as N III $\lambda\lambda 4634, 42$ emission is not visible in our spectrum, while N IV $\lambda 4058$ emission and N V $\lambda\lambda 4603, 19$ absorption are both considerably stronger than in BI 237. The EW of NIV $\lambda 4058$ is nearly three times stronger in BI 253, with the line having an EW of about -450mÅ. He I λ 4471 is *not* detectable, although this could simply be due to the poorer S/N of this spectrum compared to that of BI 253 (225 vs 500). We feel confident in placing an upper limit of 25mÅ on its presence, requiring $\log W' < -1.5$, as the EW of He II $\lambda 4542$ is 710mÅ. C IV $\lambda 4658$ emission is present (EW=-160mÅ) in comparable intensity to that of BI 237. The star's absolute magnitude ($M_V = -5.5$) is consistent with the dwarf designation suggested by the appearance of He II $\lambda 4686$. We describe the spectrum as O2 V((f*)), consistent with Walborn et al. (2002) notation, although we note that the lack of N III $\lambda 4634, 42$ emission makes the use of the "f" designation arguable.

The fitting was against straightforward (Fig. 13b), although only a lower limit could be set on the effective temperature (and hence on other stellar parameters) due to the lack of an unambiguous detection of He I $\lambda 4471$. The mass-loss rate is somewhat greater in BI 253 than it is in BI 237.

LH101:W3-14.—Both LH101:W3-14 and LMC2-675 (discussed below) are stars whose spectra are moderately early ($\sim$ O5) according to the HeI/He II ratio, but which show nitrogen features typical of much earlier stars. Are these stars spectral composites, or nitrogen-enriched objects? We have previously shown that when a star is a spectral

composite we can seldom match the actual He I and He II line strengths with a single model. The star was classified as O3 V by Testor & Niemela (1998), and then reclassified as ON5.5 V((f)) by Massey et al. (2000) based on the spectrum used here. The Testor & Niemela (1998) spectrum of this star is clearly noisy (see their Fig. 4), and it is not clear whether or not He I absorption is present in their spectrum or not. It is certainly present in ours, at a strength typical of an O5 star, with a value of $\log W'$ equal to -0.49. Here we also see (Fig. 14) N IV λ4058 and N III $\lambda\lambda$ 4634,42 emission of comparable intensity, so if we were to ignore the He I absorption spectrum we would conclude that the star was O3 V((f*)) according to the criteria of Walborn et al. (2002). N V $\lambda\lambda 4603, 19$ absorption is also weakly present, characteristic of an early spectral type. On the other hand, the presence of C III λ4650 absorption is typical of a later spectral type (O8.5+). The absolute visual magnitude of the star, $M_V = -5.6$, is somewhat brighter than the $M_V = -5.2$ value listed by Conti (1988) for an O5 dwarf, and is more consistent with a giant classification. The strength of He II λ4686 absorption is weaker than that of He II λ4542, and so a giant designation is not precluded. Alternative, the absolute magnitude may be suggesting that the object is the composite of two dwarfs.

The modeling quickly demonstrated to our satisfaction that this spectrum is composite. A 40,000 K model can match the line strengths of the He II lines and that of He I λ4387, but this model's He I λ4471 line is then many times stronger than what is actually observed. (This goes in the *opposite* sense of the "dilution effect" described by Repolust et al. 2004.) We can achieve the correct line *ratio* for He I λ4387 and He I λ4471 by lowering the effective temperature to 38,000 K, but the He I line *strengths* are then much greater than what is actually observed, and the He II lines are too weak. This is consistent with a composite spectrum, with an O3 V dominating the nitrogen and He II spectrum, and a latter O-type dominating the He I spectrum. We further note that the He I λ4471 line appears to be broader ($v \sin i = 130$ km s^{-1}) than the He II lines ($v \sin i = 110$ km s^{-1}), a difference that

is quite noticeable with our S/N and dispersion.

LH101:W3-19.—This star was classified as O3 If by Testor & Niemela (1998) and again as O3 If* by Massey et al. (2000); the data for the latter are the same as what are used here. Using the criteria suggested by Walborn et al. (2002) the star would have to be considered of spectral type O2 If*, as the N IV λ4058 emission (EW=-300mÅ) is greater than the N III $\lambda\lambda$463442 emission (EW=-230mÅ). (Fig. 15a). The presence of weak C IV λ4658 emission (EW=-150mÅ) suggests it is quite hot. N V $\lambda\lambda 4603, 19$ absorption and Si IV $\lambda\lambda 4089, 4116$ emission are clearly visible. He II λ4686 is in strong emission rather than P Cygni emission, attesting that it is a supergiant and not a giant. supergiant classification is consistent with the high absolute visual magnitude, $M_V = -7.04$, found for this star.

We have *HST* and ground-based data for both the blue part of the spectra and Hα. Nebulosity is strong around this star, and the *HST* data proved crucial for the Hα region. Although the *HST* data in the blue give less contaminated Balmer lines, the S/N is so much worse (130 vs. 420 per 1.4Å) that we used the ground-based data for the fitting, but made checked that the *HST* data yielded similar results.

The fitting of this star was relatively straightforward, with reasonably good fits. The surface gravity of the star is somewhat higher than what we might naively expect for a supergiant, with $\log g = 3.9$. The inferred spectroscopic mass is very high, $> 190 M_\odot$, one of the highest known. He I λ4471 may be *marginally* detected, with an EW of 50mÅ (and $\log W' \sim -1.1$); we were unable to convince ourselves whether or not this feature was real, and we therefore treat the effective temperature as a lower limit.

LMC2-675.—This star was classified as "O3 If+O" by Massey et al. (1995), who recognized its composite nature. The spectrum of this star (Fig. 16) is very similar in appearance to that of LH101:W3-14 (Fig. 14), with a He I to He II ratio suggesting a spectral type O5, but with strong N features that would be characteristic of an earlier

type. Our modeling confirms that this object is a composite. No model simultaneously fits the strengths of the He I and He II lines. In this case we find we can match the He II lines and He I λ4387 line with a single model of temperature 40,000 K, but that the He I λ4471 line from the model is much too strong. Furthermore, the He II lines are shifted in radial velocity by about 30 km s^{-1} relative to those of He I and H. The strength of N IV λ4058 emission and N V $\lambda 4603, 19$ absorption, plus the absence of any N III $\lambda 4634, 42$ emission would suggest that one of the components is an O2 giant [i.e., O2 III(f*)]. The other component must be an O-type dwarf. Note that for the earliest types (O2-3.5) the absolute visual magnitude is not a good indicator of luminosity class, as argued in Paper I, so this need not be in conflict with the relatively modest $M_V = -5.0$.

3.1.3. The R136 Stars

The R136 cluster in the LMC contains more extreme O-type stars than are known in total elsewhere (Massey & Hunter 1998). For an interesting subsample of stars, the FOS "classification quality" spectra of Massey & Hunter (1998) have been supplemented by higher resolution STIS spectra with considerably greater S/N for the purposes of modeling. Since the STIS spectra cover only the wavelength region from Hγ to He II λ4542 (plus a separate exposure at Hα; see Sec. 2), we make use of the FOS spectra in determining the spectral type, but use only the STIS data for the modeling. The model spectra for the He II λ4686 line are, however, compared to the FOS data for this line. In presenting the blue-optical spectra. we have spliced in the better STIS data in the wavelength region 4310Å to 4590Å.

R136-007.—This star was classified as O3 If*/WN6-A by Walborn & Blades (1997); Massey & Hunter (1998) agreed with this spectral type. The spectrum is shown in Fig. 17a. As noted earlier, the "slash" designation simply denotes strong Of-like emission. Walborn

et al. (2002) specifically excluded such "slash" stars from their discussion, but to us this division seems arbitrary and unnecessary The absorption spectrum is straightforwardly interpreted as O2-O3 given the strong He II λ4542 and lack of detection of He I λ4471. Based upon the nitrogen emission spectrum, we would classify the star as O2 If*, as N IV λ4058 emission is much stronger than N III $\lambda\lambda 4634, 42$ emission. C IV λ4658 emission is also present, suggesting this is particularly hot O2 star. The presence of N V $\lambda\lambda 4603, 19$ absorption and Si IV $\lambda\lambda 4089, 4116$ emission is also consistent with this designation. The EW of He II λ4686 is -7Å, well short of the -10Å (arbitrary) boundary between WRs and Of stars. Its absolute visual magnitude $M_V = -6.9$ is similar to that of the O2 If* star LH101:W3-19 discussed above, and is consistent with a supergiant designation.

We had difficulty matching the depth of the hydrogen and He II lines with our modeling, and are forced to conclude that this star is a composite. Indeed, Massey et al. (2002) found light variations of this star that are indicative of eclipses.

R136-014.—This star was classified as O4 If by Melnick (1985), under the designation Mk37) and as O4 If+ by Massey & Hunter (1998). Although He I λ4471 is *weakly* present in our STIS spectrum, the EW is only 40mÅ, and it is difficult to see how it could have been unambiguously detected in these earlier studies. We derive a value of $\log W' = -1.0$, suggesting a type earlier than O4. Walborn et al. (2002) reclassify the star (under the name "MH14") as O3.5 If*, given the equal strengths of the N IV λ4058 and N III $\lambda\lambda 4634, 42$ emission lines. The He II λ4686 line has an EW of -7Å, and the star's absolute magnitude, $M_V = -6.4$, is consistent with it being a supergiant (Conti 1988).

The fits were relatively straightforward, and the comparison between the model and observations are shown in Fig. 18b. Note that although the He II λ4686 was not used in the process, the agreement between the model and the observation is quite good.

R136-018.—This star was classified as O3 III(f*) by Massey & Hunter (1998), and this

spectral type was repeated by Walborn et al. (2002). We show the spectrum in Fig. 19a. He I λ4471 is present with an EW of 90mÅ; we measure $\log W' = -0.87$. NIV λ4058 is present in emission (EW=-750mÅ), although NIII $\lambda\lambda 4634, 42$ is not; the N emission lines would therefore allow either an O2 or O3 classification according to Walborn et al. (2002), while the strength of He I would argue for the later type. The strength of He II λ4686 absorption and overall weakness of the nitrogen emission spectra argues that the star is a dwarf or giant rather than a supergiant. Its absolute magnitude, $M_V = -5.9$, is intermediate between that expected for a dwarf and a supergiant (Conti 1988), and so we retain the O3 III(f*) classification.

The fitting of this star required only two model runs to obtain an excellent fit; we show the agreement between the observation and model spectrum in Fig. 19b. The surface gravity is found to be consistent with a giant.

R136-033.—This star was classified as O3 V by Massey & Hunter (1998). He I λ4471 is marginally detected, with an EW$\sim$ 50mÅ and $\log W' = -1.2$. By the "old" criteria, we would call this spectral subtype O3. Neither N IV λ4058 nor N III $\lambda\lambda 4634, 42$ emission is detectable in our FOS spectrum, and so it is difficult to know how to apply the criteria suggested by Walborn et al. (2002) based upon the relative intensities of these lines. (We will return to issue in general in Sec. 4.) For now, we will call the star an O2-3.5 V. The absolute magnitude $M_V = -5.1$ is consistent with the star being a dwarf.

The fitting for this star was also straightforward, and the results are shown in Fig. 20b. The surface gravity for this star is found to be similar that of R136-018 ($\log g = 3.75$), despite the fact that R136-033 is a dwarf and R136-018 is a giant. We note in Sec. 5 that there is no clear distinction in the surface gravities of giants and dwarfs in general among the earlier O stars. We list its parameters in Table 5 as if the presence of He I λ4471 were real, but possibly these should be viewed as upper limits.

3.2. Agreement with Other Wavelength Regions

3.2.1. Far Ultraviolet

Some studies of the physical properties of O-type stars have relied solely on the ultraviolet region for modeling (see, for example, Garcia & Bianchi 2004, Bianchi & Garcia 2002, Pauldrach et al. 2001), while other recent studies have included both the optical and ultraviolet regions in their modeling efforts (for instance, Crowther et al. 2002, Hillier et al. 2003, Bouret et al. 2003). In general the UV provides the much-needed diagnostics of the stellar wind lines (particularly the terminal velocities) but the various lines that have been proposed as particularly temperature sensitive (for example, C III λ1176 to C IV λ1169 by Bouret et al. quoting S. R. Heap in preparation, Fe IV to Fe V by Hillier et al. 2003, Ar VI λ1000 to Ar VII λ1064 by Taresch et al. 1997, etc.) are usually useful over a very limited temperature range, and, more importantly, good matches between the model and stellar spectra require determining the abundances of the particular element. The lines in the UV region are also not particularly sensitive to the surface gravity; see discussion in Pauldrach et al. (2001). Nevertheless, it would clearly be instructive to perform a detailed analysis of the UV spectra of the stars in our sample, given the good quality *HST*/STIS spectra plus the availability of *FUSE* data for several stars, and we plan to address this in a future paper. For now, we will restrict our attention to how consistent our optical and *HST*/FUV fits are to the spectrum in the "farther" ultraviolet region revealed by our *FUSE* data. In particular, we expect that the O VI $\lambda\lambda 1032, 1038$ doublet will provide a critical check on our determination of the terminal velocities, something which we will make use of in Sec. 5.2.

There are five stars in our sample for which we have *FUSE* data. Of these, one star is composite (AV 476), and two stars have only lower limits determined for the effective temperatures (Sk$-67°22$ and BI 253). For the remaining stars, AV 177 and Sk$-65°47$, we adopt the stellar parameters from Table 5 as the preliminary input to WM-BASIC

However, the formation of the O VI line is dependent upon the soft x-rays and EUV radiation produced by shocks in the stellar winds; see discussion in, for example, Pauldrach et al. (1994). Accordingly we found that we needed to "model" the O VI line in the sense of adjusting the x-ray luminosity until the line was sufficiently strong. Although there are other adjustable parameters of the shocks (Pauldrach et al. 1994, 2001) we find the resulting synthetic spectrum of the O VI line to be relatively insensitive to their exact values, in accord with the discussion in Sec. 4.2 of Pauldrach et al. (2001). In order for any meaningful comparison, we must also account for the interstellar features, and we are indebted to L. Bianchi for computing these for the appropriate color excesses. Let us consider the two stars in turn.

For AV 177 we found that in order for WM-BASIC to reproduce our measured values of the mass-loss rate and terminal velocity we had to significantly increase the surface gravity of the star from the $\log g$ value of 3.8 determined in our FASTWIND modeling to a value of 4.1. The alternative approach would have been to have varied the force multipliers to values that are inconsistent with radiatively-driven wind theory (see Kudritzki et al. 1989, Pauldrach et al. 1990, and Pauldrach et al. 1994). With $\log g$ thus increased, we then varied the force multipliers k from 0.090 to 0.124 and α from 0.474 to 0.618 (δ fixed to 0.10) to obtain a mass-loss rate of $0.3 \times 10^{-6} M_{\odot}$ yr^{-1} and three values of v_{∞} roughly bracketing our derived value of 2650 km s^{-1}. We see in Fig. 21 that there is relatively good agreement with our modeled O VI profile and that observed; the best value of v_{∞} would be about 2400 km s^{-1}, or about 250 km s^{-1} lower than our modeling of the C IV and N V lines would indicate. The models were run with $\log L_X/L_{\star} = -8.5$.

We were, of course, disturbed by the large value of $\log g$ needed for the standard stellar-wind law to match the observed terminal velocity of this star. We investigated this further, and found that AV 177 stands out as an exception amongst our program objects.

Could we simply have underestimated the surface gravity in our FASTWIND fitting? In Fig. 22 we show the change in the for Hγ and Hδ line profiles that occurs between a $\log g$ value of 3.8 (red) and 4.1 (green). Clearly $\log g$ of 3.8 is the better fit, and we can exclude the higher value from the optical lines.

For Sk$-65°47$ we found that we could increase the surface gravity negligibly from $\log g = 3.6$ to 3.65 and obtain good values for $\dot{M}$ and v_∞ with only slight changes in the force multiplier parameters. We varied the k from 0.20 to 0.24, and varied α from 0.58 to 0.62 in order to obtain a mass-loss rate of $1.2 \times 10^{-5} M_\odot$ yr $^{-1}$ (from Table 5), and values of v_∞ of 1830 to 2100 km s^{-1}. As shown in Fig. 23, the best value is about 2000 km s^{-1}, quite similar to the 2100 km s^{-1} we measure from the C IV line. The models used a "best fit" of $\log L_{\rm X}/L_\star = -6.2$.

We conclude from this examination of the O VI profiles two things. First, there is relatively good agreement between the terminal velocities we obtain from modeling the C IV λ1550 doublet and that we obtain from modeling the O VI λ1036 doublet. Although the C IV line is highly sensitive to the terminal velocity, it is observationally more challenging to observe in the FUV, and there is the additional complication of correcting for interstellar absorption. Secondly, this exercise has reemphasized the need to examine the *entire* observable region in evaluating how well determined the stellar parameters are. Although the fitting of lines in the UV is relatively insensitive to $\log g$ (Pauldrach et al. 2001), the requirement that the force multipliers parameters be sensible does impose additional constraints on $\log g$ as we show in our analysis of AV 177. We believe that there is much to be gained by fitting the UV *and* optical region, as has been shown in the past by some (see in particular Taresch et al. 1997), but has generally been ignored by others. Although the present paper (and Paper I) has made some *use* of the UV (in terms of determining the terminal velocity), our study has been wedded to that of the optical lines, as these lines

have the greatest sensitivity to $\log g$ and $T_{\rm eff}$. Nevertheless, the UV region contain differing ion states of various metal lines that can be effectively employed. The most robust answers will come from fully utilizing both the optical and UV, and we plan to make further use of our beautiful UV spectra (both *HST* and *FUSE*) in a subsequent paper.

3.2.2. The NUV: He I λ3187 *and He II* λ3203

In Paper I we (re)introduced the He I λ3187 and He II λ3203 lines as an interesting check on the models and effective temperatures we adopt. Morrison (1975) was the first to call attention to the usefulness of these lines, noting that the He II λ3203 (n=3-5) line was the only accessible He II line that did not involve transitions from $n = 4$. The He I λ3187 line is a triplet 2^3S-4^3P^o, similar to λ4471 (2^3P^o-4^3D).

Of the six stars in this paper for which we have observations in the NUV region, two are composites. In Fig. 24 we show the spectra of the other four. Although we did not use this region in determining the physical parameters of these stars, in all four cases there is good agreement between the observed spectra and the models for He II λ3203. In Paper I we also demonstrated good agreement for the two stars for which we had NUV data. We conclude that the He II λ3203 line yields answers which are consistent with that of He II λ4200 and λ4542. None of the stars were sufficiently late for He I λ3187 to be detected at our S/N, consistent with the output of the stellar atmosphere models. Since He I λ4471 and, in some cases, even He I λ4387 is measurable in all of these stars (with the possible exception of LH101:W3-19; see Sec. 3.1), we note that while the NUV region provides reassurance on our fitting procedure, the additional information added is limited.

4. The Earliest O Stars

Although the main goal of our paper is to derive physical parameters, we have assembled some of the highest quality optical spectra on some of the earliest O stars known, and we would be remiss to not use this to comment upon the spectral classification scheme. Conti & Alschuler (1971) provided equivalent width measurements of the primary spectral classification lines He I λ4471 and He II λ4542 for a large sample of O stars that had been classified in the "traditional way" (staring at photographic spectra and comparing the spectra of program stars to the spectra of spectral standards) and provided a *quantitative* scale which could be used to distinguish the spectral subtypes from one another; i.e., an O8 spectral type had a value of $\log W'$ = EW (He I λ4471) / EW (He II λ4542 between 0.10 and 0.19, while an O8.5 star had a value of $\log W'$ between 0.20 and 0.29. This scheme was slightly revised for the earliest types by Conti & Frost (1977), who used the criteria that O4 stars have $\log W' < -0.60$ while in O3 stars He I λ4471 is "absent". (A summary of the $\log W'$ appears in Table 1-3 of Conti 1988.) Of course, this leads to a the O3 classification as being degenerate; i.e., at a given surface gravity, stars with any temperature above some value might be classified as "O3". Indeed, when higher signal-to-noise spectrograms were obtained by Kudritzki (1980) and Simon et al. (1983) of the prototype O3 stars HD 93205, HD 93128, and HD 303308 (Walborn 1971a, 1973b), weak He I λ4471 was revealed, with EWs of 75-250 mÅ, and $\log W'$= -1.1 to -0.5. (HD 303308, with a $\log W' = -0.5$, would today be classified as an O4 star; see Table 3 of Walborn et al. 2002. Another O3 star for which Simon et al. 1983 detected He I λ4471 is HD 93129A, but today we recognize that this is a composite spectrum; see Nelan et al. 2004.) However, to date no one has actually provided a quantitative distinction in the He I/He II ratio between spectral types O3 and O4.

Walborn et al. (2002) attempted to partially alleviate the O3 degeneracy problem by

using the N IV λ 4058 and N III $\lambda 4634, 42$ emission lines to extend the spectral classification to spectral type O2 ("N IV >>> N III") with the introduction of an intermediate type (O3.5) for which N IV $\sim$ N III. (The O2 class would then be the degenerate subtype.) The classification criteria are not quantitative, and the system still relies upon statements such as "very weak He I" or "no He I" as secondary criteria. The criticism has been made (both here and in Paper I) that relying upon the relative strengths of the optical nitrogen lines lacks a solid theoretical underpinning; i.e., although a unique spectral subclass may be defined, it is not clear that the stars that effective temperature is the primary thing that distinguishes O2's from O3's in this scheme. The mechanism for N III emission in O stars has been well described by Mihalas & Hummer (1973), who demonstrated the N III $\lambda 4634, 42$ lines will come into emission even in a static, non-extended atmosphere if the effective temperature is sufficiently high, due to a complicated NLTE effect. Thus the presence of N III $\lambda 4634, 42$ in dwarfs and giants should be related to effective temperature. However, for stars with significant mass-loss rates, an additional process known as the Swings mechanism (Swings 1948) will come into play, enhancing the N III emission (see discussion in Mihalas & Hummer 1973). No such detailed analysis exists for the N IV $\lambda 4058$ line, although Tarsesh et al. (1997) show its behavior as a function of effective temperature holding the surface gravity constant and maintaining the same Hα profile by slightly varying the mass-loss rate. Indeed, the Tarsesh et al. (1997) analysis of HD 93129A showed the power of using the N III and N IV emission lines as a constraint on the effective temperature, *if* other parameters (such as $\log g$ and $\dot{M}$) were constrained by other observations.

In order to provide a more quantitative assessment of the classification criteria, in Table 6 we provide for the first time equivalent width measurements and ratios for the He I $\lambda 4471$/He II $\lambda 4542$ absorption lines, and N III $\lambda 4634, 42$ / N IV $\lambda 4058$ emission lines, for a sample of the earliest O-type stars. We have classified the stars using the Walborn et

al. (2002) criteria; otherwise, all of the stars earlier than O4 would simply be described as "O3". Some of the dwarfs in Paper I had no detected N III *or* N IV emission and were simply called "O3 V"; here we "revised" the type to "O2-3.5 V". (The need to detect these lines, which are weak or non-existent in dwarfs, particularly at low metallicities, is an obvious draw back to the new classification criteria.)

First, let us note that the dividing line between O3's and O4s occurs at roughly a $\log W' = -0.8$, and we would propose this as an improvement over the old description that He I be "absent". However, even a casual inspection of Table 6 shows the effect that mass-loss has on the derived effective temperature for a given He I/He II ratio. LH101:W3-24, an O3 V((f+)) star, and BI 237, an O2 V((f*)) star, both have similar $T_{\rm eff}$ and $\log g$, although their He I/He II ratios differ by a factor of 6! This can be readily attributed to the significantly greater mass-loss rate of BI 237 due to its larger radius, mass, and luminosity. (Recall from the discussion in Paper I and here that the effect of wind-blanketing will be to *decrease* the derived effective temperature for a given HeI/HeII ratio, in part because of the filling in of HeI due to emission produced in the stellar wind.)

In Fig. 25a, we show the relationship between the HeI/HeII and NIII/NIV ratios. There is a reasonable correlation in this figure, in that stars of a given luminosity class which have a small HeI/HeII ratio (right side of the diagram) also tend to show a smaller NIII/NIV emission line ratio (top of the diagram). The correlation is quite good for the dwarfs (filled circles), with giants (triangles) and supergiants (open circles) exhibiting more scatter. To us this is as expected. Although HeI absorption is affected by stellar winds (by the filling in of emission), the strength of the nitrogen *emission* lines are likely to be more affected by an extended atmosphere.

We address this in a more quantitative way in Fig. 26 where we show the correlation of effective temperature with (a) the HeI/HeII ratio and (b) the NIII/NIV ratios. Again, this

considers only the earliest-type O stars. For the dwarfs (filled circles) there are very large changes in both HeI/HeII and NIII/NIV with little change in effective temperature. In other words, although the extension of the spectral classification through O2-O3.5 for the dwarfs is unwarranted in terms of effective temperature. For the giants (denoted by triangles) and supergiants (open circles) there is more of a correlation of effective temperature with either spectroscopic criteria, but neither is very good. Consider, for example, the star with the *hottest* temperature in our sample, LH64-16. An independent analysis (using the optical spectrum, however) yielded a similar effective temperature (Walborn et al. 2004) as what we derived in Paper I. However, the giant R136-018 has a NIII to NIV emission ratio which is at least as small, but has nearly the *coolest* effective temperature for any of the giants with a measured NIII/NIV ratio in our sample! (Recall from the discussion above that the lack of NIII emission in the spectrum of R136-018 would allow either an O2 or O3 designation; the argument for the O3 classification came about from the strength of He I absorption.)

It is also worth noting that the spectroscopic luminosity criteria proposed for the earliest types (based upon wind criteria) do not prove to be a reliable indicator of the effective surface gravities. Although the supergiants in Table 6 do have lower surface gravities than the dwarfs, one cannot differentiate the dwarfs and giants on the basis of $\log g$. We return to this point in Sec. 5.

Thus in terms of the *physical properties* of early-type O stars, and in particular the effective temperatures, we are forced to conclude that there is little benefit to the extension to spectral type O2 proposed by Walborn et al. (2002). For a star of the same effective temperature and similar surface gravity either the HeI/HeII ratio or the NIII/NIV ratio can vary by essentially the full range found between O2 and O3.5 (for example, BI 237 and LH101:W3-24). We believe that careful *modeling* of the N III and N IV emission lines, in concert with other lines will provide useful diagnostics (following Tarsesh et al. 1997), but

our work here suggests that it is naive to expect that the line ratios give one insight into the effective temperature of the star. On the other hand, we note that the He I/He II line ratio doesn't fair much better. *Although the earliest O-type stars (what would have classically been called "O3") contain stars with a significant range of effective temperatures, no one spectroscopic diagnostic (such as the He I/He II or N III/N IV line ratios) provides a good clue as to the effective temperature without knowledge of the other physical parameters (mass-loss rate, surface gravity).*

5. Results

With the work described here and Paper I, we have attempted to model the spectra of 40 O-type stars in the Magellanic Clouds. We succeeded for 13 SMC stars (8 dwarfs, 2 giants, and 3 supergiants) and 20 LMC stars (9 dwarfs, 4 giants, and 7 supergiants), with the other 7 stars showing signs of composite spectra. This sample is now large enough for us to determine preliminary effective temperature scales for O stars in the SMC and LMC, and compare these to that of the Milky Way, using the sample of stars analyzed by by Repolust et al. (2004) using the same methods and models atmospheres. We also wish to make good on our promise in Paper I to examine the modified Wind Momentum Luminosity relation from these new data, and, finally, to compare the spectroscopically derived stellar masses with those derived from stellar evolutionary tracks.

In Table 8 we summarize the derived parameters for our final sample of 33 stars. In what follows we assume the fitting errors as quoted in Paper I, namely an uncertainty of about 1000 K (2-3%) in $T_{\rm eff}$, 0.1 dex in $\log g$, and 20% in $\dot{M}$. In general our values for v_∞ are good to 100 km s^{-1} (5%). Using the propagation of errors analysis by Repolust et al. (2004) [see their equation 8] we would then expect the uncertainty in the derived stellar radius R to correspond to $\Delta \log R \sim 0.03$, or about 7%, where we have allowed for a 0.1 mag

uncertainty in M_V. (The uncertainty in the radii of Galactic stars is about twice as great, given the much greater uncertainty in the distances and hence a larger uncertainty in M_V.) The total luminosity of the star is uncertain by about 0.12 mag in M_{bol}, or 0.05 in $\log L/L_\odot$.

For the stars with only lower limits on $T_{\rm eff}$ we expect that the values for the stellar radii, $D_{\rm mom}$, and $M_{\rm spect}$ are all *approximately* correct; nevertheless, we do not use them in the analysis, in order not to mix good values with bad.

In Fig. 27 we show the location of our stars in the H-R diagram, where we have over-plotted the evolutionary tracks of the Geneva group (i.e., Charbonnel et al. 1993 for the SMC, and Schaerer et al. 1993 for the LMC). For simplicity we show only the H-burning part of the tracks. Since the time of these calculations various improvements have been made in the evolutionary code, such as the inclusion of the Vink et al. (2000, 2001) prescription for mass-loss, improved opacities, and, most importantly, the inclusion of the effects of rotation. However, a full set of these tracks are not available for low metallicities. We do show the new tracks (for an initial rotation velocity of 300 km s^{-1}) for initial masses of $60M_\odot$ and $40M_\odot$ from Meynet & Maeder (2004); we are grateful to Georges Meynet for making these tracks available to us.

5.1. Effective Temperatures, Surface Gravities, and Bolometric Corrections

In Fig. 28 we show the effective temperatures as a function of spectral subtype for the complete data set: SMC stars are shown in green, the LMC in red, and the Milky Way in black, with different symbols representing the various luminosity classes. Due to the constraints of limited observing time, and our emphasis on trying to understand the effect that metallicity has on the physical parameters of stars, our LMC sample (intermediate metallicity) is incomplete, but biased towards the earliest spectral types, while the SMC

stars (low metallicity) was chosen to cover the full range of spectral subtypes for direct comparison with the Milky Way sample of Repolust et al. (2004).

First, we can see from Fig. 28 that both in the Milky Way and in the SMC that the effective temperatures of supergiants are 3000 to 4000 K cooler than dwarfs of the same spectral types for early O stars (O4-O6). For stars of spectral type O8 and later, there is essentially no difference in the effective temperatures of dwarfs and supergiants. In both galaxies the giants (denoted by triangles) appear to follow the same sequence as the dwarfs (filled circles). For the early O stars (O4-O6) SMC stars are roughly 4000 K hotter than their Galactic counterparts. By spectral type O8 the difference is about 2000 K, and by O9.5 the data are consistent with no difference. Thus, by coincidence the effective temperature scale of SMC *supergiants* is very similar to that of Milky Way *dwarfs*.

This is consistent with what we expect by way of the effects that stellar winds will have on the effective temperature scale of stars: at higher temperatures, stars with high luminosities (supergiants) will have higher mass-loss rates than stars of lower luminosity (dwarfs). At higher metallicities (Milky Way) the mass-loss rates will be higher than at lower metallicities (SMC). By the later spectral types (O8-B0) the differences should become relatively minor, as these stars have weaker stellar winds.

The LMC data on the earliest spectral types (O2-O3.5) emphasizes again how diverse a group of stars these are. Nevertheless, some clear patters emerge, and in particular the fact that the supergiants are significantly ($\approx$ 5000 K) cooler than dwarfs of similar spectral types.

With these trends in mind, we provide in Table 7 a provisional effective temperature scale for the three galaxies. Owing to the lack of data points for intermediate and late LMC O stars, we have adopted values for the LMC which are intermediate for that of the SMC and Milky Way; what limited data we do have (i.e., spectral type O5 in Fig. 28)

supports this. We emphasize that this scale is not the final word on the subject; indeed, we were in a quandary as to what effective temperatures to assign for the O3-O4 class where the the SMC dwarfs in our sample have a lower effective temperature scale than the O5 Vs; we chose to assign a higher temperature than our analysis of AV 177 and AV 378 would indicate. (We remind the reader that AV 177 also showed an inconsistency in the $\log g$ value needed to match the wind parameters than that indicated by the fitting of the Balmer lines; possibly this star is peculiar.) The effective temperature scales can be made more trustworthy by observations and analysis of LMC stars of all luminosity classes at intermediate and late O-type, and SMC stars of the earliest types. A third priority but much needed would be studies of stars of additional O and early-B type in the Milky Way to complement the Herculean efforts of Repolust et al. (2004).

We present the adopted temperature scale in Fig. 29(a). We include for comparison the Vacca et al. (1996) scale for Galactic stars, which is much hotter; the scales are shown in comparison to the data in Figs. 29(b) and (c).

We were initially surprised to find that the effective temperature scales for giants and dwarfs were indistinguishable, but an inspection of the surface gravities in Table 8 reveals the reason: in general, there is no difference in the surface gravities derived for these stars, except for the two latest types. In our sample this might be due to the fact that all but these two giants are of early type (O2-3.5) where, as we have previously emphasized, the physical properties are not obviously correlated with the details of the spectral properties. However, even for the Galactic stars studied by Repolust et al. (2004) there is only a modest difference found in the surface gravities of dwarfs and giants, with averages of 3.7 (dwarfs) and 3.6 (giants) found from their Table 1. Conti & Alschuler (1971) note that in the original MK system luminosity classes were defined for O stars only for the O9 subclass, and this was based upon the strength of ratio of Si IV $\lambda 4089, 19$ to He I $\lambda 4143$ (see Morgan

et al. 1943). Subsequently, Walborn (1971b) used the N III $\lambda 4634, 42$ emission lines and the He II $\lambda 4686$ line (either absorption or emission) to establish luminosity classification criteria. As we have previously noted, these lines are not gravity-sensitive *per se* but rather may reflect the effects of surface abundances, effective temperatures, and what is happening in the stellar winds (both mass-loss rate and density/temperature profiles) in a complicated manner. It is clear the the supergiants (both in the Milky Way and in the Magellanic Clouds) have lower surface gravities than do the stars spectroscopically classified as dwarfs, but there is so far no evidence to support that the early- or mid-type giants (defined primarily as having "weakened "He II $\lambda 4686$ absorption) as having lower surface gravity than the dwarfs. Theoretical modeling that includes the N III $\lambda 4634, 42$ line will help address this important issue.

However, for now let us note a particularly egregious example, namely the star LH64-16. Walborn et al. (2002, 2004) make a point of declaring this the prototype of the O2 giant class. Yet, compare its physical properties to the O2 dwarfs BI 253 and BI 237. LH64-16 may be hotter, but the three stars have the same surface gravities, similar stellar radii, mass-loss rates, and bolometric luminosities. The spectral appearance of LH64-16 differs from that of BI 253 and BI 237 primarily in the fact that the He II $\lambda 4686$ shows more of a P Cygni profile in LH64-16, plus the nitrogen lines (N IV and N III emission, and N V absorption) are significantly stronger than in BI 237 and BI 253. The only physical difference we can discern between the two stars is one of chemical abundances (Paper I and Walborn et al. 2004). In Paper I we speculated that perhaps this star is the product of binary evolution. We return to this in Sect. 5. In any event, the luminosity criteria used by Walborn et al. (2002) in this case do not seem to be tied into the properties one usually uses to distinguish amongst the second MK dimension, such as actual luminosity.

How does our effective temperature scale compare to that from other recent studies

using line-blanketed models? We give the comparison in Fig. 30. For the supergiants (Fig. 30a) we see that the agreement is modest. The WM-BASIC modeling of Galactic supergiants by Bianchi & Garcia (2002) and Garcia & Bianchi (2004) is consistently lower in $T_{\rm eff}$ than our analysis of early and mid-type O supergiants. The FASTWIND study of Cyg OB2 stars by Herrero et al. (2002) is unsurprisingly in better agreement, although their data would suggest our Galactic scale should be hotter for the earliest supergiants and cooler for the latest. More interesting is the disagreement with the CMFGEN studies of Crowther et al. (2002). Here the data for the Magellanic Cloud stars would indicate a considerably hotter scale than what we find. However, an analysis with CMFGEN by Hillier et al. (2003) of a single SMC supergiant indicates a considerably lower temperature. (Crowther et al. 2002 find a temperature of 39000 for the O7 Iaf star Sk 80, while Hillier et al. 2003 find a temperature of 32800 for the O7 Iaf star AV 83.) As discussed earlier, Puls [REFERENCE?] has found a problem with the He I singlets lines produced by CMFGEN, and until this is resolved and the same data re-analyzed it is hard to know what to make of these differences.

For the dwarfs and giants (Fig. 30b) the situation is more clear cut, with the FASTWIND modeling indicating higher effective temperatures than other recent studies. For the Galactic stars the WM-BASIC modeling by Bianchi & Garcia (2002) and Garcia & Bianchi (2004) find temperatures that are about 4000 K cooler than the mean relationship we derive from the Repolust et al. (2004) data. (The single giant modeled with FASTWIND by Herrero et al. 200) agrees with this mean relationship Galactic relationship.) The WM-BASIC modeling by Bianchi & Garcia (2002) and Garcia & Bianchi (2004) involves careful fitting of the absolute strengths of UV metal lines, such as C IV $\lambda 1169$, C III $\lambda 1176$, P V $\lambda\lambda 1118, 1128$, Si IV $\lambda\lambda 1123, 1128$, etc. In Paper I we note that the *flux distributions* of FASTWIND and WM-BASIC models agree well despite the former's use of approximate line-blanketing and blocking. We do not have a ready explanation for the systematic

difference apparent between the parameters derived by the WM-BASIC and FASTWIND modeling. However, we believe that the first step in investigating this is to use FASTWIND modeling on the optical spectra of the same stars studied by Bianchi & Garcia (2002) and Garcia & Bianchi (2004), and to model the UV spectra of the Repolust et al. (2004) using WM-BASIC and to try to understand the differences. We alluded to the need for such a complete modeling effort in Sec. 3.2.1.

More central to the current study is the difference apparent in Fig. 30b between our mean relationship for SMC dwarfs and that found by a combination of TLUSTY/CMFGEN modeling by Bouret et al. (2003). Although we cannot directly account for the difference, we will note that the physical parameters derived by Bouret et al. (2003) are less consistent with our knowledge of star formation and stellar evolutionary theory. The stars they studied are all in the NGC 346. Using what became the Chlebowski & Garmany (1991) effective temperature scale, Massey et al. (1989) derived an H-R diagram for this cluster which was highly coeval, with an age of 2-4 Myr and a typical age spread of 1 Myr (see also Massey 1998, 2003). The H-R diagram shown by Bouret et al. (2003) [their Fig. 12] reveals a systematic trend of age with spectral type; the earliest (an O2 III) shows an age of < 1 Myr, with mid-O stars showing ages of 3-4 Myr, and later O stars ages of 5.5 Myr and 12 Myr. (The latter belongs to the O9.5-B0 V star NGC346-MPG12, which Walborn et al. 2000 argue is nitrogen strong and located on the edge of the cluster; possibly this star is not associated with the cluster [3].) Indeed, the very young age (< 1 Myr) one would deduce

[3]Note that although Bouret et al. (2003) incorrectly attribute the source of the photometry used in constructing their H-R diagram to Walborn (2000), it was actually that of Massey et al. (1989); i.e., both studies started with the same UBV values, and the differences in the H-R diagrams due purely to the different effective temperature scales and slight differences in the treatment of reddenings. See below for more on the latter point.

for the O2 III star (NGC346-MPG355) would necessitate it being a zero-age main-sequence star, rather than a giant, although Bouret et al. (2003) fail to comment on this discrepancy. Massey et al. (1989) do classify the star as a dwarf, but with the older effective temperature scale find it coeval with the rest of the cluster.

In Fig. 31 we compare the H-R diagrams constructed using the Bouret et al. (2003) parameters with that made using the effective temperature scale and bolometric corrections given here. For consistency we have used the reddenings and spectral types adopted by Bouret et al. (2003) in making this comparison[4]. The effective temperature scale we adopt here lead to more consistent ages for the stars in the cluster. While this hardly proves our scale is right, and the Bouret et al. (2003) values wrong, it does emphasize an often overlooked point, namely that changes in the effective temperature scale of O stars do have implications in the interpretation of H-R diagrams and star-formation in clusters; see discussion in Hanson (2003) and Massey (2003). We plan a re-analysis of the NGC 346 stars using FASTWIND.

In Fig. 32 we show the BCs as a function of effective temperatures. As was the case with unblanketed models, there is no apparent difference with surface gravity, as is shown

[4]It should be noted that the intrinsic colors used by Bouret et al. (2003) lead to low values for the reddenings of the earliest stars, $E(B-V) = 0.05$ to 0.12. Massey et al. (1989) find a somewhat greater color excess (0.09 to 0.15). By comparison to other early-type stars in the SMC, the reddening of the early O stars in NGC 346 is average or slightly high, as might be expected; Massey et al. (1995) find an average reddening of 0.09 for the SMC. Were the Bouret et al. (2003) intrinsic colors correct, then many of the early-type stars in the SMC would have reddenings less than the expected foreground reddening to the SMC (Schwering & Israel 1991, Larsen et al. 2000). The Bouret et al. (2003) values also lead to a progression in reddenings with spectral type.

by the small scatter. There *is* a slight shift with metallicities, with stars of low metallicity (SMC) having a BC which is perhaps 3-4% larger (in the sense of being more significant) than the higher metallicity (Milky Way) stars. We find a relationship

$$\mathrm{BC} = -6.90 \times \log T_{\mathrm{eff}} + 27.99 \tag{2}$$

fit the data with an RMS of 0.03 mag. This is very similar to that found by Vacca et al. (1996) considering unblanketed models.

5.2. The Wind Momentum-Luminosity Relationship

Kudritzki et al. (1995) introduced the *modified Wind momentum Luminosity Relation (WLR)*, where

$$D_{\mathrm{mom}} \equiv \dot{M} v_{\infty} R_{\star}^{0.5} \propto L^{x}, \tag{3}$$

where $x = 1/\alpha_{\mathrm{eff}} = 1/(\alpha - \delta)$, (Puls et al. 1996). The force multipliers α and δ have been described by Kudritzki et al. (1989): α would equal 1 in the case that only strong lines contributed to the line acceleration force, and would equal 0 if only weak lines contributed. Typical values are 0.5 to 0.7 (Kudritzki 2002). The parameter δ describes the ionization balance of the wind, and typically has a value between 0.0 and 0.2 (Kudritzki 2002). Since the value of α_{eff} is expected to have only a weak dependence upon the effective temperature and metallicity (and in a way that can be theoretically predicted from radiative-driven wind theory; see Kudritzki 2002, as well as Vink et al. 2000, 2001) one can in fact use Eq. 3 to find the distances to galaxies using basic physics combined with quantitative spectroscopy of the bright supergiants.

In Fig. 33(a) we show the WLR for the stars in our sample in comparison to the Galactic sample studied by Repolust et al. (2004). Although there is considerable scatter, it is clear that the SMC stars show a lower value for D_{mom} than do the Galactic stars, with

the LMC stars being somewhat intermediate. A more subtle effect is that the supergiants of a given galaxy seem to lie somewhat higher than do the dwarfs and giants.

We can reduce the scatter in this diagram significantly by correcting the mass-loss rates given in Table 8 for "clumpiness" in the stellar wind. Repolust et al. (2004) argue that since the FASTWIND ignores the effects that inhomogeneities will have upon the Hα profiles, that the derived mass-loss rates should be decreased by a factor of 0.44 *if* the Hα profile is dominated by emission, where the numerical factor was determined empirically by forcing Galactic supergiants to follow the same WMR as do the dwarfs and giants. We indicate the stars with Hα emission in Table 8; all of the LMC supergiants are affected, but none of the SMC stars. Thus only three LMC stars are affected, after we eliminate the stars with lower limits values on $T_{\rm eff}$. We show the revised plot in Fig. 33(b). Indeed the supergiants in the LMC are in better accord with the dwarfs, just as Repolust et al. (2004) found for the Galactic stars.

In general, the SMC stars have a considerably smaller $D_{\rm mom}$ than do the Galactic stars. What would we expect on theoretical grounds?

Vink et al. (2001) calculates that for O-type stars,

$$\dot{M} \propto Z^{0.69},$$

if the Leitherer et al. (1992) relation

$$v_\infty \propto Z^{0.13}$$

is taken into account. We can therefore expect that

$$D_{\rm mom}(Z) \propto Z^{0.82}.$$

If α remained constant, we would then expect that the *slopes* in Fig. 33(b) would be the same for all three galaxies, but that the *intercepts* would be -0.25 dex lower for the LMC

than for the Milky Way, and -0.57 dex lower for the SMC than for the Milky Way. We show these relationships in Fig. 33(b), where we have adopted the Vink et al. (2001) slope and intercept as given by Repolust et al. (2004) for the Milky Way stars. We consider the agreement excellent in this diagram. Kudritzki (2002) has performed careful calculations of the effects of metallicity and effective temperature on the force multipliers, and his calculations show that at an SMC-like metallicity that α will be 3% ($T_{\rm eff} \approx 40000$ K) and 15% ($T_{\rm eff} \approx 50000$ K) larger at an SMC-like metallicity than in the Milky Way. We would thus expect x to be somewhat smaller for the SMC, and the relationship slightly more shallow, which is certainly not excluded by our data.

In evaluating Fig. 33 one should keep in mind the typical errors discussed above, i.e., an uncertainty of 0.05 dex in $\log L/L_\odot$ for the Magellanic Cloud objects, and of 0.15 for the Galactic objects. The error in $\log D_{\rm mom}$ is about 0.15 dex for both the Magellanic Cloud and Galactic objects. We show the typical error bars in the figure. Most of the stars follow the relationship fine; the notable exception is the star AV 14, which shows an upper limit of $D_{\rm mom} = 28.15$ at $\log L/L_\odot = 5.85$.

5.3. Comparison of Spectroscopic and Evolutionary Masses

The analyses of our stars have yielded values for the "spectroscopic mass", $M_{\rm spect} = (g_{\rm true}/g_\odot)R^2$ given in Table 8. We remind the reader that these $g_{\rm true}$ values have resulted from a modest correction for centrifugal acceleration to the measured $g_{\rm eff}$ values obtained from the model fits. It is of interest to compare these values with the mass $M_{\rm evol}$ which we derive from stellar evolutionary models based upon a star's $\log L$ and $T_{\rm eff}$. This comparison is shown in Fig. 34. We have included error bars, with the uncertainty in the evolutionary mass assumed to be due purely to the uncertainty in $\log L/L_\odot$ (i.e., $\Delta \log M_{\rm evol} = -0.2\Delta M_{\rm Bol}$; see equation 4 of Massey 1998). These evolutionary masses were

derived from the "standard" (non-rotating) models using the older opacities; we return to this point below.

We see that most of the stars in our sample cluster around the mean relationship $M_{\rm spect} \sim M_{\rm evol}$, but that both samples contain a fair number of objects in which the evolutionary mass which is considerably greater than the spectroscopic mass. This *mass discrepancy* was first found by Herrero et al. (1992) for Galactic stars. This problem was investigated by many authors; comparison with the masses determined from binaries have tended to support the evolutionary masses (Burkholder et al. 1997; Massey et al. 2002). The lowering of the effective temperatures for Galactic supergiants has resulted in decreasing, if not eliminating, the discrepancy for Galactic stars (Herrero 2003, Repolust et al. 2004). The expected reason is two-fold: first, lower effective temperatures imply a smaller luminosity of a star, and hence the deduced evolutionary mass will be less. Secondly, the new line-blanketed models resulted in larger radiation pressure, so a higher surface gravity is needed to reproduce the Stark-broadened wings of the Balmer lines.

Although the Galactic mass discrepancy was considerably worse for Galactic supergiants than dwarfs, we see that the discrepant stars in Fig. 34 include both dwarfs and giants, and an inspection of Table 8 suggests that the problem stars are all the stars with $T_{\rm eff} > 45000$ K, and that all stars in this temperature regime show a significant mass discrepancy. (The two stars with $T_{\rm eff} > 45000$ in the Galactic sample of Repolust et al. 2004 did not show a similar problem.)

In determining the evolutionary masses we have relied upon the older tracks of Charbonnel et al. (1993) for the SMC and Schaerer et al. (1993) for the LMC. The effects of newer tracks, including the effects of an initial rotation speed of 300 km s^{-1}, is shown in Fig. 27 by the dotted lines for the $60 M_\odot$ and $40 M_\odot$ tracks. We see that the inclusion of rotation will have a modest effect on the deduced masses compared to the non-rotating

models. For the hotter stars the effect will be to make the evolutionary masses lower; at cooler temperatures (on the main-sequence) the effect is in the other direction.

For some of the discrepant stars in Fig. 34 use of the newer evolutionary models could potentially bring the evolutionary masses into closer agreement with the spectroscopic masses. However, the effect is small compared to the high temperature mass discrepancy we note: for stars near the ZAMS, the difference is about 0.25 mag, which is equivalent to 0.05 dex in $\log M$, or about 10%

It is possible that the objects with large mass discrepancies in Fig. 34 represent the results the results of binary evolution. A good candidate is LH64-16, discussed in Paper I. This "O2N III" star shows highly processed material at the surface (Paper I and Walborn et al. 2004), and in Paper I we argue that this star might be the result of binary evolution. We note that this star is found to the left of the ZAMS in Fig. 27. A similar location was found for some of the relatively close binaries in the R136 cluster by Massey et al. (2002).

However, we are also left with the possibility that at high $T_{\rm eff}$ the models may be underestimating either $\log g$ or R. We are reminded of the fact that the star AV 177 required a higher surface gravity than that obtained by fitting the Balmer lines in order to reproduce the observed values of v_∞ and $\dot{M}$ with standard values for the force multiplier parameters; on the other hand, this star also has a lower effective temperature than one might expect from its spectral type, and so may be peculiar in some way. Further investigation is underway.

6. Summary, Conclusions, and Future Work

We have analyzed 40 O-type stars in the Magellanic Clouds, including many stars of the earliest type. Modeling was successful for 33 of these stars, with the other 7 showing

the spectroscopic signature of unresolved companions. This study, in combination with an analysis of 24 Galactic stars by Repolust et al. (2004), using similar techniques and the same model atmosphere code, allow us to obtain the following results:

1. The effective temperatures of O3-O7 dwarfs and giants in the SMC is about 4000 K hotter than for stars of the same spectral type in the Milky Way. The differences decrease as one approaches B0 V. This is readily understood in terms of the *decreased importance* of line- and wind-blanketing at the lower metallicity that characterizes the SMC. The results for the LMC appear to be intermediate between the two galaxies. A similar effect is seen for the supergiants, although the differences decrease more rapidly with increasing spectral type (i.e., Table 7 and Fig. 28). For each galaxy, there is no difference in the effective temperatures of dwarfs and giants of the same spectral type, while the supergiants are about 4000 K cooler than the dwarfs for the hottest types in the SMC, and about 6000K cooler than the dwarfs for the hottest types in the Milky Way. The differences in effective temperatures between supergiants and dwarfs decrease for the later O-types stars. Our effective temperature scale for dwarfs is significantly hotter than found by line-blanketed modeling by others, but ours would appear to lead to more consistent results with stellar evolutionary theory as evidenced by comparisons of the degree of coevality of stars in the NGC 346 cluster (i.e, Fig. 31).

2. Our data suggest that the modified wind momentum ($D_{\rm mom} \equiv v_\infty \dot{M} R^{0.5}$) scales with luminosity in the expected way with metallicity as predicted by radiatively driven wind theory (Kudritzki 2002, Vink et al. 2001):

$$D_{\rm mom} \propto L^{1/\alpha_{\rm eff}},$$

with $\alpha_{\rm eff} \approx 0.55$ fairly insensitive to $T_{\rm eff}$ or Z, and with the constant of proportionality

scaling with $Z^{0.82}$. One of the SMC stars (AV 14) with low mass-loss rates does not fit this relationship well, but most of the others do.

3. Most of the stars in our sample show a reasonable match between the spectroscopic mass and the evolutionary mass. However, stars with $T_{\rm eff} > 45000$K show a systematic difference, with the spectroscopic mass significantly less (by a factor of 2 or more) than the evolutionary mass. This is similar to the long-standing "mass discrepancy" found by Herrero et al. (1992) for Galactic supergiants, but which has now been mostly resolved due to the lower effective temperatures of the Galactic models with the effects of line-blanketing included. Use of newer evolutionary tracks (which contain improved opacities, better treatment of mass-loss, and the effects of rotation) will tend to decrease the discrepancy, but such improvement is likely to be only of order 10%, and will not account for the factors of 2 discrepancies. We are left with the conclusion that the surface gravities or stellar radii may be underestimated in our models for stars of the highest effective temperatures.

4. We find that there is little correlation in the *physical properties* (such as $T_{\rm eff}$) with the new spectral types O2-3.5. Although stars in this group contain the hottest stars, neither the NIII/NIV emission line ratio nor even the He I/He II absorption line ratio provides a clear indication of the star's effective temperature. The obvious explanation is that at these extreme spectral types the mass-loss plays a significant role in affecting these spectral diagnostics. Thus although we can predict a star's effective temperature from its two-dimension spectral type and metallicity for O4s and later, it requires a detailed analysis of the entire spectrum to derive a reliable effective temperature (i.e., the mass-loss rate inferred from Hα and the terminal velocity of the wind from UV measurements are needed in addition to the blue optical spectrum. Similarly, we find no differences in the physical properties of giants and dwarfs for the

O2-O3s.

5. Two of the stars with the largest radial velocities with respect to the LMC are O3 stars listed by Massey et al. (1995) as "field" stars i.e., they are found far from the nearest OB association. These provide the first compelling evidence for the origin of this field population.

We are grateful to the staffs of CTIO, *HST*, and *FUSE* for providing first-rate spectroscopic capabilities on well-functioning telescopes; we note with sadness the loss of STIS, which provided much of the crucial data in this series. We also acknowledge the strong encouragement of several of our colleagues over the years for this study, and in particular Peter Conti and Margaret Hanson. Support for *HST* programs GO-6417, GO-7739, and GO-9412 were provided by NASA through a grant from the Space Telescope Science Institute, which is operated by the Association of Universities for Research in Astronomy, Inc., under NASA contract NAS 5-26555; support for *FUSE* program C002 was similarly provided through NASA.

REFERENCES

Abbott, D. C., & Hummer, D. G. 1985, ApJ, 294, 286

Auer, L. H., & Mihalas, D. 1972, ApJS, 24, 193

Azzopardi, M., & Vigneau, J. 1982, A&AS, 30, 261

Bianchi, L., & Garcia, M. 2002, ApJ, 581, 610

Bouret, J.-C., Lanz, T., Hillier, D. J., Heap, S. R., Hubeny, I., Lennon, D. J., Smith, L. J., & Evans, C. J. 2003, ApJ, 595, 1182

Breysacher, J. 1981, A&AS, 43, 20

Breysacher, J., Azzopardi, M., & Testor, G. 1999, A&AS, 137, 117

Brunet, J. P., Imbert, N., Martin, N., Mianes, P., Prevot, L., Rebeirot, E., & Rousseau, J. 1975 A&AS, 21, 109

Burkholder, V., Massey, P., & Morrell, N. 1997, ApJ 490, 328

Charbonnel, C., Meynet, G., Maeder, A., Schaller, G., & Schaerer, D. 1993, A&AS, 101, 415

Conti, P. S. 1988, in O Stars and Wolf-Rayet Stars, ed. P. S. Conti & A. B. Underhill, NASA SP-497

Conti, P. S., & Alschuler, W. R. 1971, ApJ, 170, 325

Conti, P. S., & Frost, S. A. 1977, ApJ, 212, 728

Conti, P. S., Garmany, C. D., & Massey, P. 1986, AJ, 92, 48

Crampton, D. C., & Greasley, J. 1982, PASP, 94, 31

Crowther, P. A., Hillier, D. J., Evans, C. J., Fullerton, A. W., De Marco, O., & Willis, A. J. 2002, ApJ, 579, 774

Garcia, M., & Bianchi, L. 2004, ApJ, 606, 497

Garmany, C. D., Conti, P. S., & Massey, P. 1987, AJ, 93, 1070

Garmany, C. D., Massey, P., & Parker, J. W. 1994, AJ, 108, 1256

Hanson, M. M. 2003, ApJ, 597, 957

Haser, S. M., 1995, Ph.D. thesis, Univ.-Sternwarte der Ludwig-Maximilian

Haser, S. M., Lennon, D. J., Kudritzki, R.-P., Puls, J., Pauldrach, A. W. A., Bianchi, L., & Hutchings, J. B. 1995, A&A, 295, 136

Herrero, A. 2003, in A Massive Star Odyssey: From Main Sequence to Supernova, IAU Symp. 212, ed. K. A. van der Hucht, A. Herrero, & C. Esteban (San Francisco: ASP), 3

Herrero, A., Kudritzki, R. P., Vilchez, J. M.,Kunze, D., Butler, K., & Haser, S. 1992, A&A, 261, 209

Herrero, A., Puls, J., & Najarro, F. 2002, A&A, 396, 949

Hillier, D., Lanz, T., Heap, S. R., Hubeny, I., Smith, L. J., Evans, C. J., Lennon, D. J., & Bouret, J. C. 2003, ApJ, 588, 1039

Hummer, D. G. 1982, ApJ¡ 257, 724

Hunter, D. A., Vacca,W. D., Massey, P., Lynds, R., & Oneil, E. J. 1997, AJ, 113, 1691

Kim, S., Staveley-Smith, L., Dopita, M. A., Freeman, K. C., Sault, R. J., Kesteven, M. J., & McConnell, D. 1998, ApJ, 503, 674

Kudritzki, R. P. 1980, A&A, 85, 174

Kudritzki, R. P. 2002, ApJ, 577, 389

Kudritzki, R. P., Lennon, D. J., & Puls, J. 1995, in Science with the VLT, ed. J. R. Walsh & I. J. Danziger (Berlin: Springer-Verlag), 246

Kudritzki, R. P., Pauldrach, A., Pul, J., & Abbott, D. C. 1989, A&, 219, 205

Lamers, H. J. G. L. M., Cerruti-Sola, M., & Perinotto, M. 1987, ApJ, 314, 726

Larsen, S. S., Clausen, J. V., & Storm, J. 2000, A&A, 364, 455

Leitherer, C., Robert, C., & Drissen, L. 1992, ApJ, 401, 596

Lucke, P. 1972, Ph.D. thesis, Univ. Washington

Maeder, A., & Meynet, G. 2000, ARA&A, 38, 143

Martins, F., Schaerer, D., & Hillier, D. J. 2002, A&A, 382, 999

Massey, P. 1998, in The Stellar Initial Mass Function, 38th Herstmonceux Conference, ed. G. Gilmore & D. Howell (San Francisco, ASP), 17

Massey, P. 2002, ApJS, 141, 81

Massey, P. 2003, ARA&A, 41, 15

Massey, P., & Conti, P. S. 1977, ApJ, 218, 431

Massey, P., Bresolin, F., Kudritzki, R. P., Puls, J., & Pauldrach, A. W. A. 2004, ApJ, 608, 1001 (Paper I)

Massey, P., & Hunter, D. A. 1998, ApJ, 493, 180

Massey, P., Lang, C. C., DeGioia-Eastwood, K., & Garmany, C. D. 1995, ApJ, 438, 188

Massey, P., Parker, J. W., & Garmany, C. D. 1989, AJ, 98, 1305

Massey, P., Penny, L. R., & Vukovich, J. 2002, ApJ, 565, 982

Massey, P., Waterhouse, E., & DeGioia-Eastwood, K. 2000, AJ, 119, 2214

Melnick, J. 1985, A&A, 153, 235

Meynet, G., & Maeder, A. 2004, A&A, in press

Mihalas, D., & Hummer, D. G. 1973, ApJ, 179, 827

Moos, H. W. et al. 2000, ApJ, 538, L1

Morgan, W. W., Keenan, P. C., & Kellman, E. 1943, An Atlas of Stellar Spectra, (Chicago: Univ. Chicago Press)

Morrison, N. D. 1975, ApJ, 202, 433

Nelan, E. P., Walborn, N. R., Wallace, D. J., Moffat, A. F. J., Makidon, R. B., Gies, D. R., & Panagia, N. 2004, AJ, 128, 323

Oey, M. S. 2004, in The Local Group as an Astrophysical Laboratory, ed. M. Livio (Cambridge, Cambrdige University Press), in press, astro-ph/0307131

Oey, M. S., & Kennicutt, R. C., Jr. 1997, MNRAS, 291, 827

Pauldrach, A. W. A., Hoffmann, T. L., & Lennon, M. 2001, A&A, 375, 161

Pauldrach, A. W. A., Kudritzki, R. P., Puls, J., & Butler, K. 1990, A&A, 228, 125

Pauldrach, A. W. A., Kudritzki, R. P., Puls, J., Butler, K., & Hunsinger, J. 1994, A&A, 283, 525

Puls, J., Repolust, T., Hoffmann, T. L., Jokuthy, A. 2003, in A Massive Star Odyssey, from Main Sequence to Supernova, IAU Symp 212, ed. K. A. van der Hucht, A. Herrero, & C. Esteban (San Francisco: ASP), 61

Repolust, T., Puls, J., & Herrero, A. 2004, A&A, 415, 349

Sanduleak, N. 1969, CTIO Publ. 89

Schaerer, D., Meynet, G., Maeder, A., & Schaller, G. 1993, A&AS, 98, 523

Schild, H. & Testor, G. 1992, A&AS, 92, 729

Schwering, P. B. V., & Israel, F. P. 1991, A&A, 246, 231

Simon K. P., Kudritzki, R. P., Jonas, G., & Rathe, J. 1983, A&A, 125, 34

Slesnick, C. L., Hillenbrand, L. A., & Massey, P. 2002, ApJ, 576, 880

Swings, P. 1948, AnAp, 11, 228

Taresch, G., Kudritzki, R. P., Hurwitz, M., Bowyer, S., Pauldrach, A. W. A., Puls, J., Butler, K., Lennon, D. J., & Haser, S. M. 1997, A&A, 321, 531

Testor, G., & Niemela, V. 1998, A&AS, 130, 527

Testor, G., Schild, H., & Lortet, M. C. 1993, A&A, 280, 426

Vacca, W. D., Garmany, C. D., & Schull, J. M. 1996, ApJ, 460, 914

van den Bergh, S. 2000, The Galaxies of the Local Group (Cambridge: Cambridge Univ. Press)

Vink, J. S., de Koter, A., & Lamers, H. J. G. L. M. 2000, A&A, 362, 295

Vink, J. S., de Koter, A., & Lamers, H. J. G. L. M. 2001, A&A, 369, 574

Voels, S. A., Bohannan, B., & Abbott, D. C. 1989, ApJ, 340, 1073

Walborn, N. R. 1971a, ApJ, 167, L31

Walborn, N. R. 1971b, ApJS, 23, 257

Walborn, N. R. 1973a, ApJ, 186, 611

Walborn, N. R. 1973b, ApJ, 180, L35

Walborn, N. R. 1982, ApJ, 254, L15

Walborn, N. R. 1983, ApJ, 265, 716

Walborn, N. R. et al. 2002, AJ, 123, 2754

Walborn, N. R., & Blades, J. D. 1997, ApJS, 112, 457

Walborn, N. R., & Fitzpatrick, E. L. 1990, PASP, 102, 379

Walborn, N. R., Morrell, N. I., Howarth, I. D., Crowther, P. A., Lennon, D. J., Massey, P., & Arias, J. I. 2004, ApJ, 608, 1028

Westerlund, B. E. 1961, Uppsala Astron. Obs. Ann., 5, 1

Westerlund, B. E. 1997, The Magellanic Clouds (Cambridge: Cambridge Univ. Press0

This manuscript was prepared with the AAS LaTeX macros v5.2.

Table 1. Program Stars[a]

Name[b]	Cat ID[c]	α_{2000}	δ_{2000}	V	$B-V$	$U-B$	$E(B-V)$[d]	M_V[e]	Spectral Type[f]
AV 177	SMC-038024	00 56 44.17	-72 03 31.3	14.53	-0.21	-1.05	0.12	-4.78	O4 V((f))
AV 435	SMC-067670	01 08 17.88	-71 59 54.3	14.00	-0.06	-0.98	0.28	-5.81	O3 V((f*))
AV 440	SMC-068756	01 08 56.01	-71 52 46.5	14.48	-0.18	-1.00	0.15	-4.93	O8 V
AV 446	SMC-069555	01 09 25.46	-73 09 29.7	14.59	-0.24	-1.06	0.10	-4.66	O6.5 V
AV 476	SMC-074608	01 13 42.41	-73 17 29.3	13.52	-0.09	-0.93	0.28	-6.29	O2-3 V + comp.
Sk−67°22=BAT99-12	LMC-034056	04 57 27.47	-67 39 03.3	13.44	-0.18	-1.05	0.16	-5.53	O2 If*
Sk−65°47=LH43-18	···	05 20 54.67	-65 27 18.3	12.68	-0.13	-0.93:	0.19	-6.39	O4 If
LH58-496=LH58-10a[g]	···	05 26 44.21	-68 48 42.1	13.73	-0.23	-1.09	0.11	-5.09	O5 V(f)
LH81:W28-23	···	05 34 50.11	-69 46 32.3	13.81	-0.16	-1.13	0.15	-5.14	O3.5 V((f+))
LH90:Br58=BAT99-68[h]	···	05 35 42.02	-69 11 54.2	14.13	0.49	-0.48	0.85	-6.98	O3If/WN6
LH90:ST2-22	···	05 35 45.26	-69 11 35.1	13.93[i]	+0.18[i]	-0.73[i]	0.60	-6.41	O3.5 III(f+)
BI 237	LMC-164942	05 36 14.68	-67 39 19.3	13.89	-0.12	-0.97	0.25	-5.38	O2 V((f*))
BI 253	LMC-168644	05 37 34.48	-69 01 10.4	13.76	-0.09	-1.02	0.25	-5.50	O2 V((f*))
LH101:W3-14=ST5-52[j]	···	05 39 05.41	-69 29 20.7	13.41	-0.15	-0.89	0.17	-5.60	O3 V + O V Composite
LH101:W3-19=ST5-31	···	05 39 12.20	-69 30 37.6	12.37[i]	-0.06[i]	-0.92[i]	0.30	-7.04	O2 If*
LMC2-675	···	05 43 13.00	-67 51 16.0	13.66	-0.25	-1.14	0.07	-5.04	O2 III(f*) + O V Composite
R136-007=Mk39[k]	···	05 38 40.3186	-69 06 00.172	13.01	···	···	0.47	-6.9	O2 If* Composite
R136-014=Mk37[k]	···	05 38 42.4986	-69 06 15.396	13.57	···	···	0.48	-6.4	O3.5 If*
R136-018[k]	···	05 38 44.2211	-69 05 56.954	13.91	···	···	0.42	-5.9	O3 III

Table 1—Continued

Name[b]	Cat ID[c]	α_{2000}	δ_{2000}	V	$B-V$	$U-B$	$E(B-V)$[d]	M_V[e]	Spectral Type[f]
R136-033[k]	···	05 38 42.2106	-69 06 00.988	14.43	···	···	0.35	-5.1	O3 V

[a]Coordinates and photometry are from Massey 2002 or Massey, Waterhouse, & DeGioia-Eastwood 2002 unless otherwise noted.

[b]Identifications are as follows: "AV" from Azzopardi & Vigneau 1982; "BI" from Brunet et al. 1975; "BAT" from Breysacher, Azzopardi, & Testor 1999; "Br" from Breysacher 1981; "LH" from Lucke 1972 except as noted, "LMC2" from Massey et al. 1995 and Massey 2002; "Sk" from Sanduleak 1969; "ST" from Testor & Niemela 1998; "W" from Westerlund 1961; "Mk" from Melnick 1985; "R136-NNN" from Hunter et al. 1997 and Massey & Hunter 1998

[c]Designations from the catalog of Massey 2002.

[d]From averaging the color excesses in $B-V$ and $U-B$ based upon the spectral type. See Massey 1998b.

[e]Computed using $A_V = 3.1 \times E(B-V)$, with assumed distance moduli for the SMC and LMC of 18.9 and 18.5, respectively (Westerlund 1997, van den Bergh 2000).

[f]New to this paper.

[g]H58-10A identification is from Lucke 1972; LH58-496 identification is from Garmany at al. 1994.

[h]Misidentified with a neighboring bright star in Table 4 of Massey 2002.

[i]Photometry new to this paper, based upon the CCD material described by Massey 2002.

[j]Coordinates and photometry from Testor & Niemela 1998.

[k]Coordinates and photometry from Hunter et al. 1997 and Massey & Hunter 1998.

Table 2. Sources of the Data Used in This Study

Spectral Region	Telescope	Instrument	Aperture (arcsec x arcsec)	Grating	Wavelength (Å)	Resolution (Å)
Far-UV	FUSE/C002	···	30x30	···	905-1187	0.1
UV	HST/9412	STIS	0.2x0.2	G140L	1150-1740	0.9
Near-UV	HST/9412	STIS	0.2x52	G430M	3020-3300	0.4
Blue-optical	CTIO 4-m	RC Spec	1.3x330	KPGLD	3750-4900	1.4
	HST/7739,9412	STIS/CCD	0.2x52	G430M	4310-4590	0.4
	HST/6417	FOS	0.26(circ)	G400M	3250-4820	3.0
Hα	CTIO 4-m	RC Spec	1.3x330	KPGLD	5400-7800	2.8
	HST/7739,9412	STIS/CCD	0.2x52	G750M	6300-6850	0.8

Table 3. Spectral Regions Observed

Star	FUV	UV	NUV	Blue-optical	Hα
AV 177	FUSE	HST/9412	···	CTIO 4-m	CTIO 4-m, HST/9412
AV 435	···	HST/9412	···	CTIO 4-m	CTIO 4-m, HST/9412
AV 440	···	HST/9412	···	CTIO 4-m	HST/9412
AV 446	···	HST/9412	···	CTIO 4-m	CTIO 4-m, HST/9412
AV 476	FUSE	HST/9412	···	CTIO 4-m	CTIO 4-m, HST/9412
Sk−67°22	FUSE	HST/9412	···	CTIO 4-m	HST/9412
Sk−65°47	FUSE	HST/9412	HST/9412	CTIO 4-m, HST/9412	HST/9412
LH58-496	···	HST/9412	HST/9412	CTIO 4-m	HST/9412
LH81:W28-23	···	HST/9412	HST/9412	CTIO 4-m	CTIO 4-m, HST/9412
LH90:Br58	···	HST/9412	···	CTIO 4-m	CTIO 4-m, HST/9412
LH90:ST2-22	···	HST/9412	···	CTIO 4-m	CTIO 4-m, HST/9412
BI 237	···	HST/9412	···	CTIO 4-m	CTIO 4-m, HST/9412
BI 253	FUSE	HST/9412	···	CTIO 4-m	CTIO 4-m, HST/9412
LH101:W3-14	···	HST/9412	HST/9412	CTIO 4-m	CTIO 4-m, HST/9412
LH101:W3-19	···	HST/9412	HST/9412	CTIO 4-m, HST/9412	CTIO 4-m, HST/9412
LMC2-675	···	HST/9412	HST/9412	CTIO 4-m	CTIO 4-m, HST/9412
R136-007	···	HST/9412	···	HST/7739, HST/6417	HST/7739
R136-014	···	HST/9412	···	HST/7739, HST/6417	HST/7739
R136-018	···	HST/9412	···	HST/7739, HST/6417	HST/7739
R136-033	···	HST/9412	···	HST/7739, HST/6417	HST/7739

Table 4. Terminal Velocities in km s^{-1}

Star	v_∞	Lines Used	Comments
AV 177	2650	CIV, NV	
AV 435	1500::	CIV, SiIV	Weak CIV
AV 440	1300:	CIV	Weak CIV
AV 446	1400:	CIV	Weak CIV
AV 476	2670	CIV	
Sk−67°22	2650	CIV	
Sk−65°47	2100	CIV	
LH58-496	2400::	CIV	Wide CIV, plus abs. contamination
LH81:W28-23	3050	CIV	
LH90:Br58	1900:	SiIV	Could not use CIV
LH90:ST2-22	2560	CIV	
BI 237	3400	CIV	
BI 253	3180	CIV	
LH101:W3-14	3100	CIV	
LH101:W3-19	2850	CIV	
LMC2-675	3200	CIV	
R136-007	2100	CIV, SiIV	
R136-014	2000	CIV, SiIV	Velocity scale uncertain
R136-018	3200	CIV	
R136-033	3250	CIV	

Table 5. Results of Model Fits

Name	Spectral Type	$T_{\rm eff}$ (°K)	$\log g_{\rm eff}$ [cgs]	$\log g_{\rm true}$[a] [cgs]	R ($R_\odot$)	M_V mags	BC mags	$M_{\rm bol}$ mags	Mass $M_\odot$	$\dot{M}$ ($10^{-6} M_\odot$ yr^{-1})	β	v_∞ (km s^{-1})	He/H[b]	Comments
AV 177	O4 V((f))	44000	3.80	3.85	8.9	-4.78	-4.04	-8.82	21	0.3	0.8	2650	0.15	$\dot{M} <$ 0.5
AV 435	O3 V((f*))	45000	3.80	3.81	14.2	-5.81	-4.12	-9.93	48	0.5	0.8	1500::	0.10	
AV 440	O8 V	37000	4.00	4.01	10.6	-4.93	-3.52	-8.45	42	0.1	0.8	1300:	0.12	$\dot{M} <$ 0.3
AV 446	O6.5 V	41000	4.15	4.15	8.8	-4.66	-3.82	-8.48	40	0.1	0.8	1400	0.15	$\dot{M} <$ 0.3
AV 476	O2-3 V+comp.	...	...	...	-6.29	...	...	...	...	...	2670	...	...	Composite
Sk $-67°22$	O2 If*	$>$ 42000	$\approx$3.5	$\approx$3.56	$\approx$13.2	-5.53	< -3.94	-9.47	$\approx$23	15	0.8	2650	0.30	$T_{\rm eff}$ lower limit
Sk $-65°47$	O4 If	40000	3.60	3.62	20.1	-6.39	-3.79	-10.18	61	12	0.8	2100	0.10	
LH58-496	O5 V	42000	4.00	4.04	10.5	-5.09	-3.88	-8.97	44	0.6	0.8	2400	0.10	
LH81:W28-23	O3.5 V((f+))	47500	3.80	3.81	10.0	-5.14	-4.26	-9.40	24	2.5	0.8	3050	0.25	
LH90:Br58	O3If/WN6	40000-42000:	3.5:	3.5:	30:	-6.98	-4.1::	-11.1:	100::	40:	3.0	1900	0.1::	See text
LH90:ST2-22	O3.5 III(f+)	44000	3.70	3.71	18.9	-6.41	-4.05	-10.46	67	4.5	0.8	2560	0.20	
BI 237	O2 V((f*))	48000	3.90	3.92	11.1	-5.38	-4.29	-9.67	37	2.0	0.8	3400	0.10	
BI 253	O2 V((f*))	$>$ 48000	$\approx$3.90	$\approx$3.93	$\approx$11.8	-5.50	$<$-4.30	$<$-9.80	$\approx$43	3.5	0.8	3180	0.10	$T_{\rm eff}$ lower limit
LH101:W3-14	O3 V + O V	...	...	...	-5.60	...	...	...	...	...	...	3100	...	Composite
LH101:W3-19	O2 If*	$>$ 44000	$\approx$3.90	$\approx$3.91	$\approx$ 25.5	-7.04	$<$-4.06	$<$-11.10	$\approx$193	20	0.8	2850	0.10	$T_{\rm eff}$ lower limit
LMC2-675	O2 III(f*) + O V	...	...	...	-5.04	...	...	...	...	...	...	3200	...	Composite
R136-007	O2 If* Composite	...	...	...	-6.9	...	...	...	...	...	...	2100	...	Composite
R136-014	O3.5 If*	38000	3.50	3.51	21.1	-6.4	-3.65	-10.0	53	23	0.8	2000	0.10	
R136-018	O3 III(f*)	45000	3.75	3.77	14.7	-5.9	-4.11	-10.0	46	2.0	0.8	3200	0.10	
R136-033	O2-3.5 V	47000	3.75	3.77	9.8	-5.1	-4.23	-9.3	21	2.0	0.8	3250	0.10	

[a]By number.

Table 6. Line Strengths in the Earliest O-type Stars

Star	Type	$T_{\rm eff}$ (1000 K)	$\log g_{\rm true}$ (cgs)	$\dot{M}$ ($10^{-6} M_\odot$ yr^{-1})	EWs [mÅ] He I λ4471	EWs [mÅ] He II λ4542	$\log \frac{\rm EW(HeI)}{\rm EW(HeII)}$	EWs [mÅ] N IV λ4058	EWs [mÅ] N III λ4634, 42	$\log \frac{\rm EW(NIII)}{\rm EW(NIV)}$	Comments
DWARFS											
BI 237	O2 V((f*))	48.0	3.92	2.0	20	750	−1.6	−165	−90	−0.3	C IV λ 4658
BI 253	O2 V((f*))	>48.0	≈ 3.93	3.5	<25	710	<−1.5	−450	>−60	<−0.9	C IV λ 4658
AV 435[a]	O3 V((f*))	45.0	3.81	0.5	125	750	−0.8	−80	>−60	<−0.1	
LH101:W3-24	O3.5 V((f+))	48.0	4.01	0.5	120	790	−0.8	> −20	−200	>1.0	O3 V((f)) in Pap I.
LH81:W28-23	O3.5 V((f+))	47.5	3.81	2.5	80	830	-1.0	−120	−500	0.6	
AV 177[a]	O4 V((f))	44.0	3.85	0.3	170	950	−0.8	>−50	−250	>0.7	
LH81:W28-5	O4 V((f+))	46.0	3.81	1.2	200	890	−0.7	−50	−480	1.0	
R136-055	O2-3.5 V	47.5	3.81	0.9	35	650	−1.3	>−200	>−200	···	O3 V in Paper I
R136-033	O2-3.5 V	47.0	3.77	2.0	50	790	< −1.2	>−200	>−200	···	O3 V in this paper
R136-040	O2-3.5 V	>51.0	≈3.81	2.0	<100	760	<−0.9	>−200	>−200	···	O3 V in Paper I
GIANTS											
LH64-16	ON2 III(f*)	54.5	3.91	4.0	100	1090	−1.0	−660	−120	−0.7	C III λ 4658
R136-047	O2 III(f*)	>51.0	≈3.91	6.0	<30	450	<−1.2	−700	>−250	<−0.5	
R136-018	O3 III(f*)	45.0	3.77	2.0	90	670	−0.9	−750	>−150	<−0.7	
LH90:ST2-22	O3.5 III(f+)	44.0	3.71	4.5	140	880	−0.9	−230	−750	0.5	
SUPERGIANTS											
Sk−67 22	O2 If*	>42.0	≈3.56	15	<50	650	<−1.1	−1610	−350	−0.7	C IV λ4658
LH101:W3-19	O2 If*	>44.0	≈3.91	<20	<∼50	570	< −1.1	−300	−230	−0.1	C IV λ4658
R136-020	O2 If*	>42.5	≈3.61	23	<30	510	<−1.2	−2570	>−100	<−1.4	
R136-036	O2 If*	>43.0	≈3.71	14	<50	550	<−1.0	−2020	>−200	<−1.0	
LH90:Br58	O3 If/WN6	40−42	3.5:	40:	<50	400	<−0.9	−1010	−480	−0.3	
R136-014	O3.5 If*	38.0	3.51	23	40	400	−1.0	−1360	−1400	0.0	
Sk−65° 47	O4 If	40.0	3.62	12	115	550	−0.7	−175	−1540	0.9	

Table 6—Continued

Star	Type	$T_{\rm eff}$ (1000 K)	$\log g_{\rm true}$ (cgs)	$\dot{M}$ ($10^{-6} M_\odot$ yr^{-1})	EWs [mÅ] He I λ4471	EWs [mÅ] He II λ4542	$\log \frac{\rm EW(HeI)}{\rm EW(HeII)}$	EWs [mÅ] N IV λ4058	EWs [mÅ] N III λ4634, 42	$\log \frac{\rm EW(NIII)}{\rm EW(NIV)}$	Comments

[a]SMC star.

Table 7. Effective Temperature Scale [K]

Type	Milky Way		SMC	
	V+III	I	V+III	I
O3	46500	40250	49500	45250
O4	44000	39000	47750	43000
O5	41000	37750	45000	41000
O5.5	39500	36750	43500	40000
O6	38250	36000	42250	38500
O6.5	37000	35500	41000	37500
O7	36000	34750	39250	36250
O7.5	34750	34000	37750	35250
O8	33750	33000	36250	34000
O8.5	32750	32500	34500	33000
O9	31750	31750	33000	32000
O9.5	30750	30750	31500	30750
B0	30000	29750	30000	29750

Table 8. Parameters for the Complete Sample

Star	Spectral Type	$v \sin i$ km s^{-1}	$T_{\rm eff}$ [1000 K]	$\log g_{\rm true}$ [cgs]	$\dot{M}$ [10^{-6} $M_\odot$ yr^{-1}]	v_∞ [km s^{-1}]	$R/R_\odot$	He/H [num.]	$\log D_{\rm mom}$	$\log L/L_\odot$	$M_{\rm spect}$	$M_{\rm evol}$[a]
DWARFS												
R136-040	O2-3.5 V	120	>51.0	≈3.81	2.0	3400	≈10.3	0.10	≈29.14	>5.82	≈25	>70
BI 253	O2 V((f*))	200	>48.0	≈3.93	3.5	3180	≈11.8	0.10	≈29.38	>5.82	≈43	>64
BI 237	O2 V((f*))	150	48.0	3.92	2.0	3400	11.1	0.10	29.16	5.77	37	62
R136-033	O2-3.5 V	120	47.0	3.77	2.0	3250	9.8	0.10	29.11	5.6	21	52
R136-055	O2-3.5 V	120	47.5	3.81	0.9	3250	9.4	0.10	28.75	5.6	21	52
LH101:W3-24	O3 V((f))	120	48.0	4.01	0.5	2400	8.1	0.15	28.33	5.49	25	48
AV 435[b]	O3 V((f*))	110	45.0	3.81	0.5	1500::	14.2	0.10	28.3::	5.87	48	62
LH81:W28-23	O3 V((f+))	120	47.5	3.81	2.5	3050	10.0	0.20	29.18	5.66	24	55
AV 177[b]	O4 V((f))	220	44.0	3.85	0.3	2650	8.9	0.15	28.18	5.43	21	40
LH81:W28-5	O4 V((f+))	120	46.0	3.81	1.2	2700	9.6	0.20	28.80	5.58	22	50
AV 377[b]	O5 V((f))	120	45.5	4.01	<0.3	2350	9.1	0.35	<28.13	5.52	31	45
AV 14[b]	O5 V	150	44.0	4.01	<0.3	2000	14.2	0.10	<28.15	5.85	75	59
LH58-496	O5 V	250	42.0	4.04	0.6	2400	10.5	0.10	28.47	5.49	44	41
AV 446[b]	O6.5 V	95	41.0	4.15	<0.3	1400	8.8	0.15	<27.90	5.29	40	33
AV 207[b]	O7.5 V((f))	120	37.0	3.72	<0.3	2000	11.0	0.10	<28.10	5.32	23	29
AV 296[b]	O7.5 V((f))	300	35.0	3.63	0.5	2000	11.9	0.10	28.34	5.28	22	29
AV 440[b]	O8 V	100	37.0	4.01	<0.3	1300:	10.6	0.12	<27.9:	5.28	42	30
GIANTS												
LH64-16	ON2 III(f*)	120	54.5	3.91	4.0	3250	9.4	1.0	29.40	5.85	26	76
R136-047	O2 III(f*)	120	>51.0	≈3.91	6.0	3500	≈10.4	0.10	≈28.64	>5.82	≈32	>70
R136-018	O3 III(f*)	180	45.0	3.77	2.0	3200	14.7	0.10	29.19	5.9	46	65
LH90:ST2-22	O3.5 III(f+)	120	44.0	3.71	4.5	2560	18.9	0.20	29.50	6.08	67	79
AV 378[b]	O9.5 III	110	31.5	3.27	···	···	15.4	0.15	···	5.34	17	29
AV 396[b]	B0 III	120	30.0	3.52	···	···	14.1	0.15	···	5.17	24	22
SUPERGIANTS												
LH101:W3-19	O2 If*	180	>44.0	≈3.91	20[c]	2850	≈25.5	0.10	≈30.26	>6.34	≈193	>109
R136-036	O2 If*	120	>43.0	≈3.71	14[c]	3700	≈12.8	0.10	≈30.07	>5.7	≈31	>50
R136-020	O2 If*	120	>42.5	≈3.61	23[c]	3400	≈16.4	0.20	≈30.30	>5.9	>40	>62
Sk -67 22	O2 If*	200	>42.0	≈3.56	15[c]	2650	≈13.2	0.30	≈29.96	≈5.69	>23	>49
LH90:Br58	O3If/WN6	···	40.0-42.0	3.5:	40:[c]	1900	30:	30.4	0.1::	6.3:	40:	101:
R136-014	O3.5 If*	120	38.0	3.51	23[c]	2000	21.1	0.10	30.12	5.9	53	57
Sk -65 47	O4 If	160	40.0	3.62	12[c]	2100	20.1	0.10	29.85	5.97	61	65

Table 8—Continued

Star	Spectral Type	$v \sin i$ km s^{-1}	$T_{\rm eff}$ [1000 K]	$\log g_{\rm true}$ [cgs]	$\dot{M}$[10^{-6} $M_\odot$ yr^{-1}]	v_∞ [km s^{-1}]	$R/R_\odot$	He/H [num.]	$\log D_{\rm mom}$	$\log L/L_\odot$	$M_{\rm spect}$	$M_{\rm evol}$[a]
AV 75[b]	O5.5 I(f)	120	40.0	3.61	3.5	2100	25.4	0.10	29.37	6.16	96	84
AV 26[b]	O6 I(f)	150	38.0	3.52	2.5	2150	27.5	0.10	29.25	6.14	91	81
AV 469[b]	O8.5 I(f)	120	32.0	3.13	1.8	2000	21.2	0.20	29.02	5.64	22	39

[a]From the non-rotating models of Charbonnel et al. 1993 (SMC) and Schaerer et al. 1993 (LMC).

[b]SMC

[c]Hα in emission; these values for $\dot{M}$ should be reduced by a factor of 0.44 to allow for the effects of clumping in the stellar wind. See text.

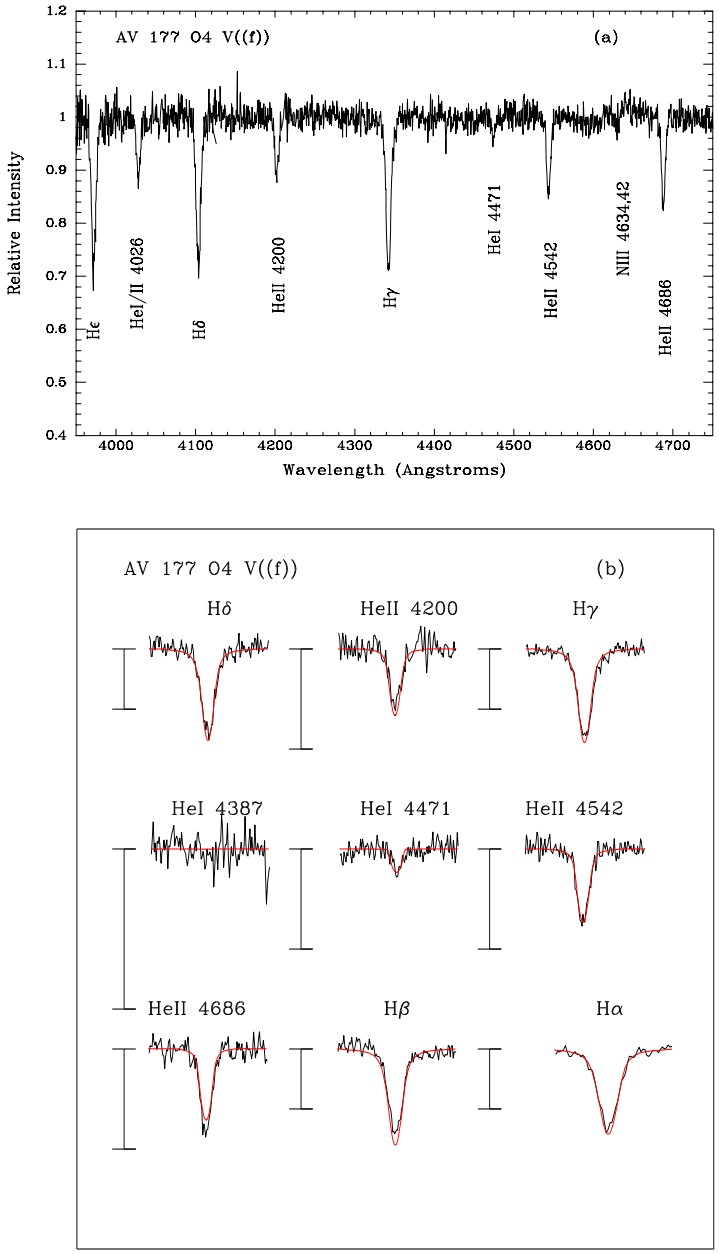

Fig. 1.— AV 177. (a) A portion of the blue-optical spectrum of AV 177 is shown with the major lines identified. (b) Selected spectral lines (black) are shown compared to the model fits (red). The bar to the left of each line shows a change of 20% intensity relative to the continuum, and the top of the bar denotes the continuum level. A radial velocity of 100 km s^{-1} and a rotational broadening $v \sin i$ of 220 km s^{-1} was used in making this comparison.

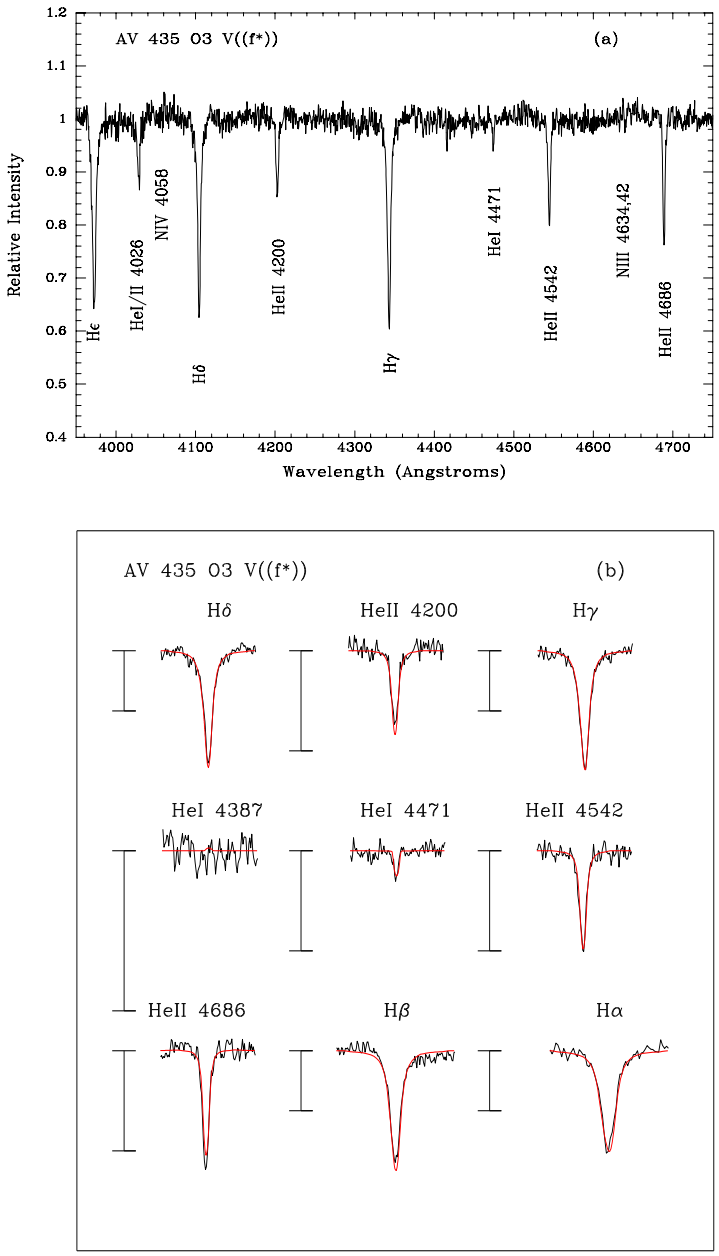

Fig. 2.— AV 435. Same as Fig. 1. A radial velocity of 200 km s^{-1} and a rotational broadening $v \sin i$ of 110 km s^{-1} was used in making this comparison.

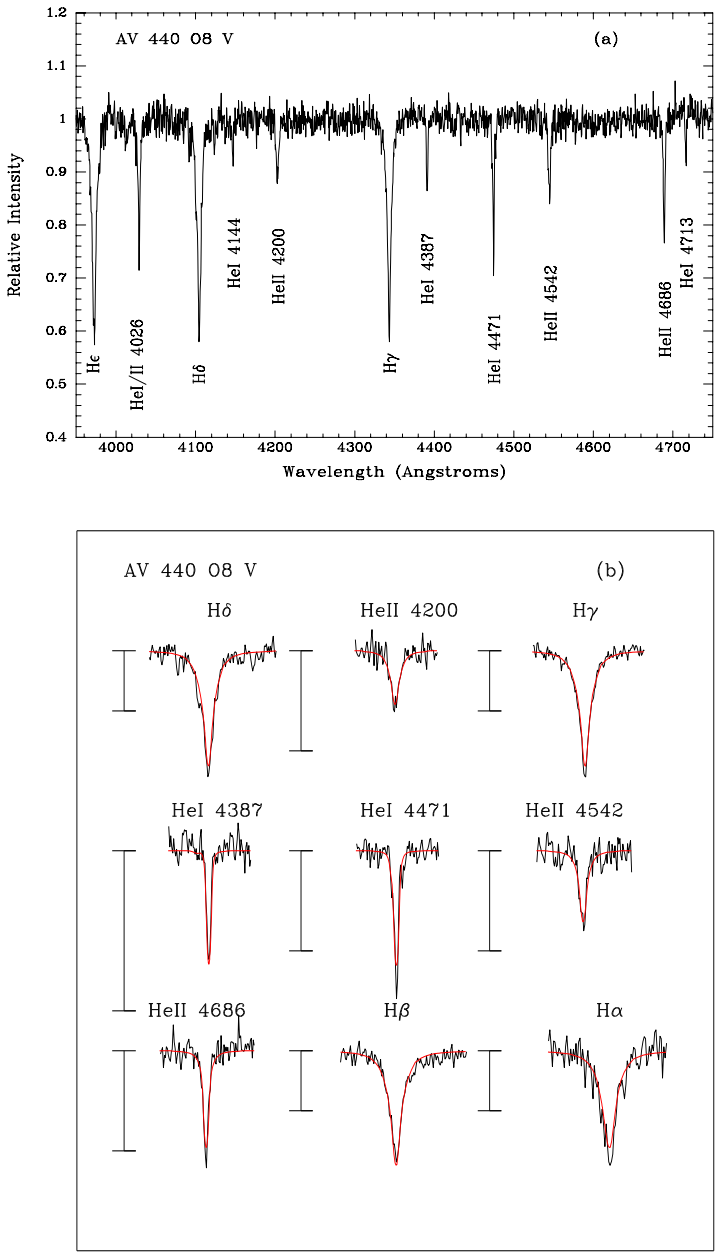

Fig. 3.— AV 440. Same as Fig. 1. A radial velocity of 190 km s^{-1} and a rotational broadening $v \sin i$ of 100 km s^{-1} was used in making this comparison.

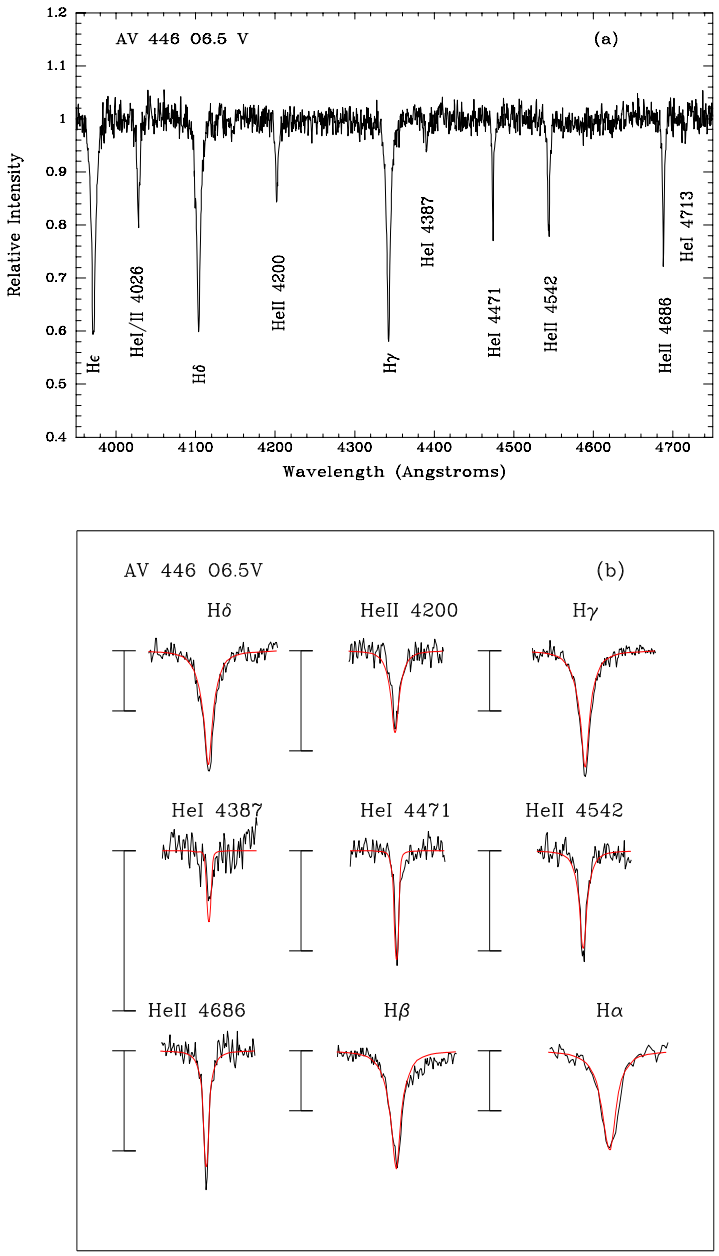

Fig. 4.— AV 446. Same as Fig. 1. A radial velocity of 140 km s^{-1} and a rotational broadening $v \sin i$ of 95 km s^{-1} was used in making this comparison.

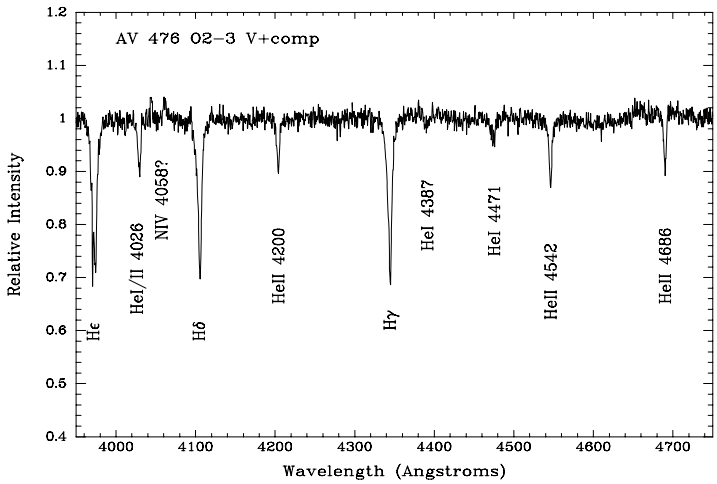

Fig. 5.— AV 476. This star shows a composite spectrum.

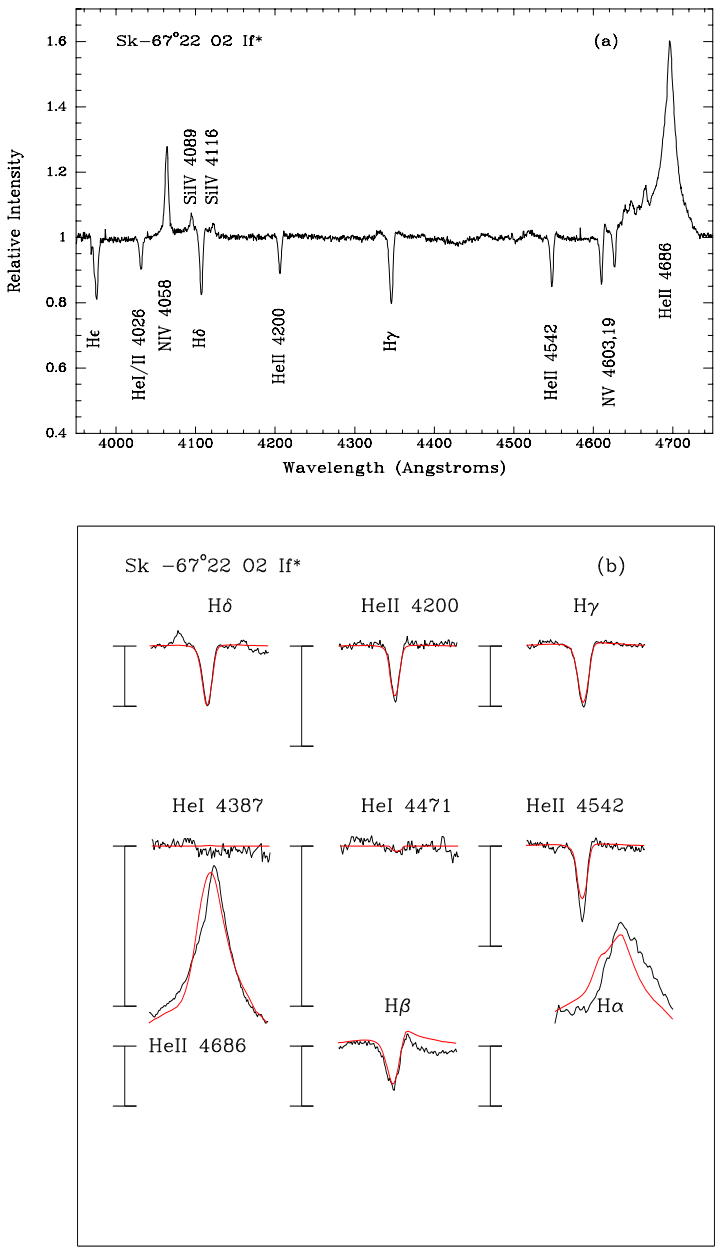

Fig. 6.— Sk−67°22. Same as Fig. 1. A radial velocity of 430 km s^{-1} and a rotational broadening $v \sin i$ of 200 km s^{-1} was used in making this comparison.

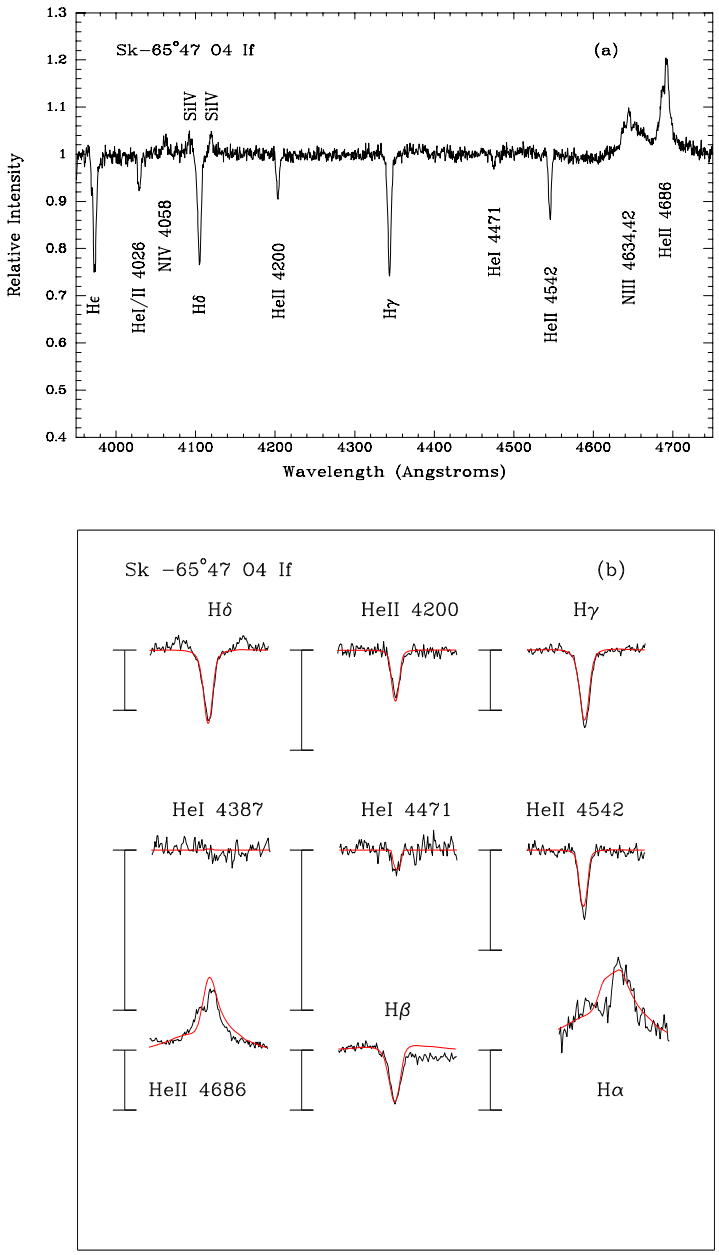

Fig. 7.— Sk−65°47. Same as Fig. 1. A radial velocity of 250 km s^{-1} and a rotational broadening $v \sin i$ of 160 km s^{-1} was used in making this comparison.

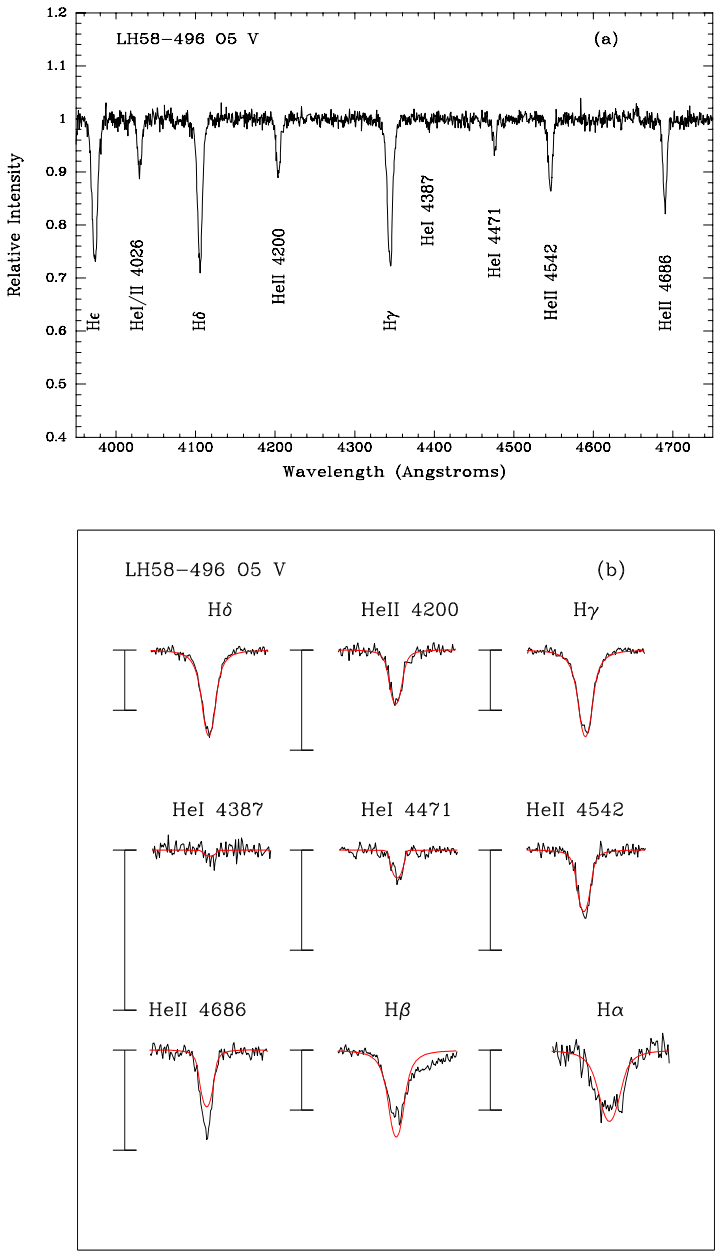

Fig. 8.— LH58-496. Same as Fig. 1. A radial velocity of 275 km s^{-1} and a rotational broadening $v \sin i$ of 250 km s^{-1} was used in making this comparison.

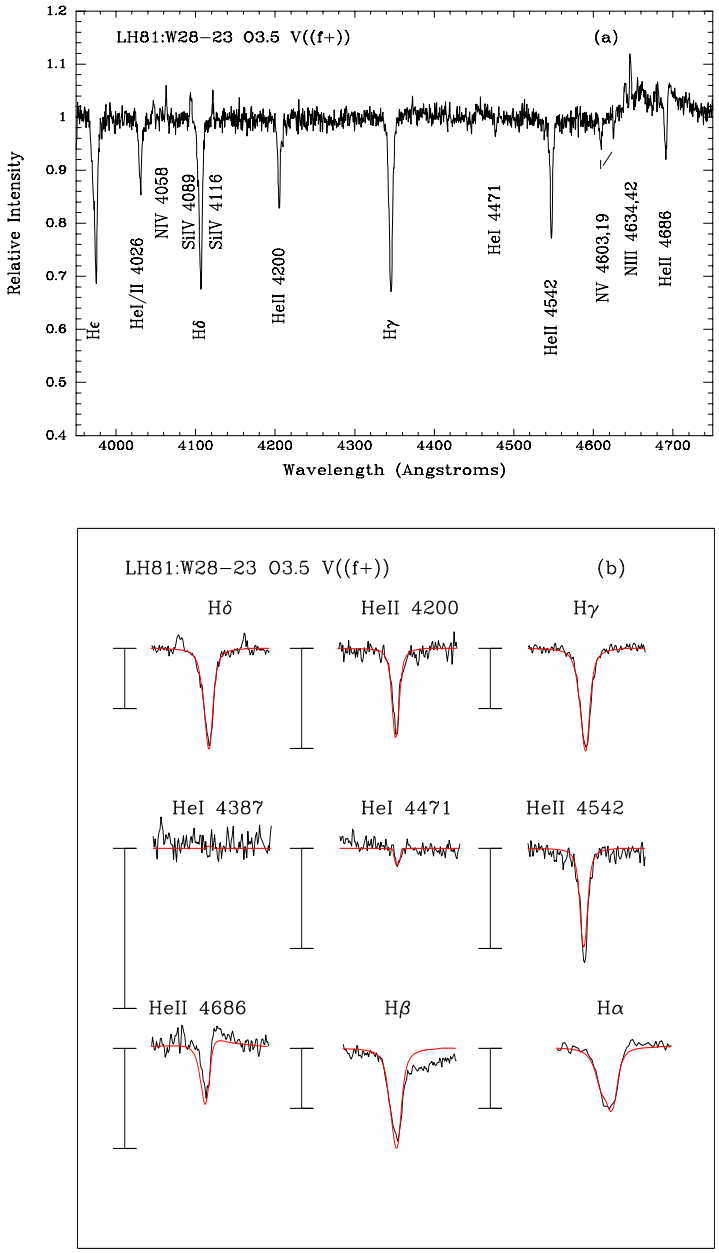

Fig. 9.— LH81:W28-23. Same as Fig. 1. A radial velocity of 350 km s^{-1} and a rotational broadening $v \sin i$ of 120 km s^{-1} was used in making this comparison. A cosmic ray on the wing of the He II λ4200 has been removed in this plot.

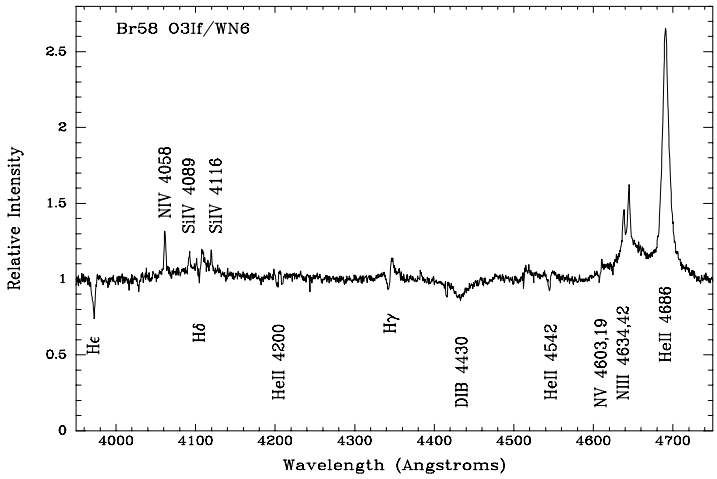

Fig. 10.— LH90:Br58. The strong emission in this star prevented a satisfactory fit, although tentative parameters are given in the text. Note the strong diffuse interstellar band at λ4430.

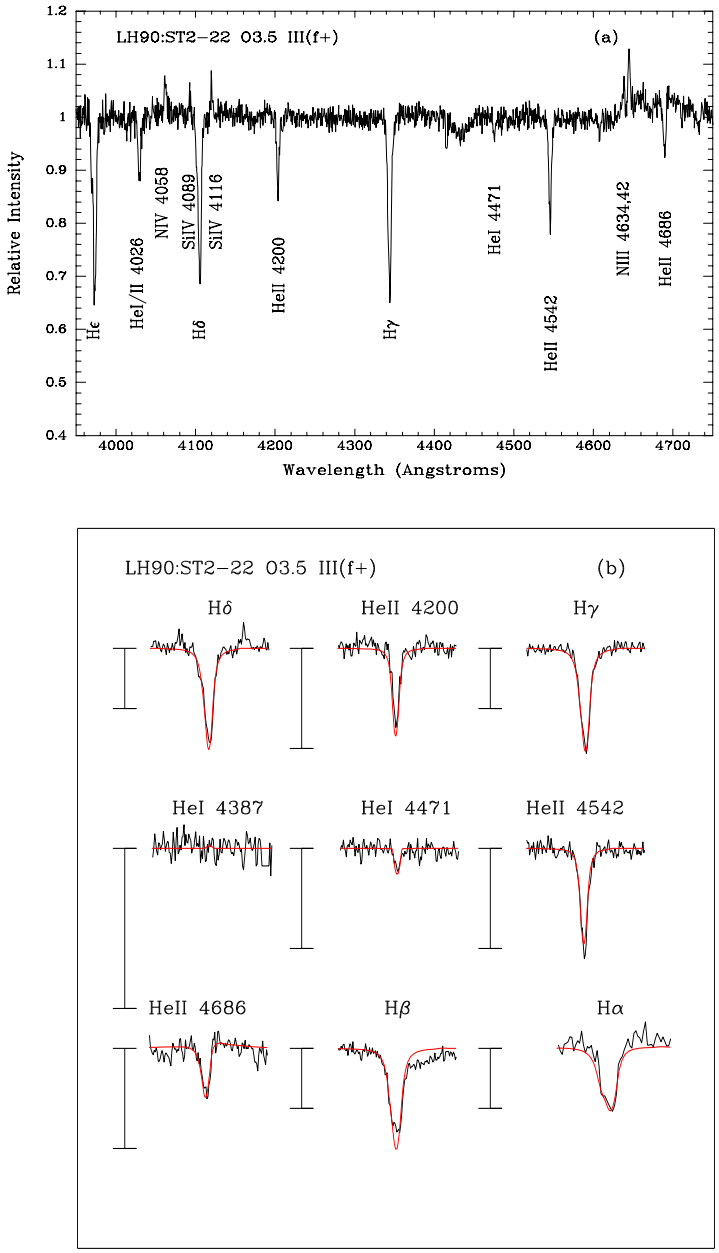

Fig. 11.— LH90:ST2-22. Same as Fig. 1. A radial velocity of 250 km s^{-1} and a rotational broadening $v \sin i$ of 120 km s^{-1} was used in making this comparison. A cosmic ray on the He II λ4200 profile has been removed in this fit.

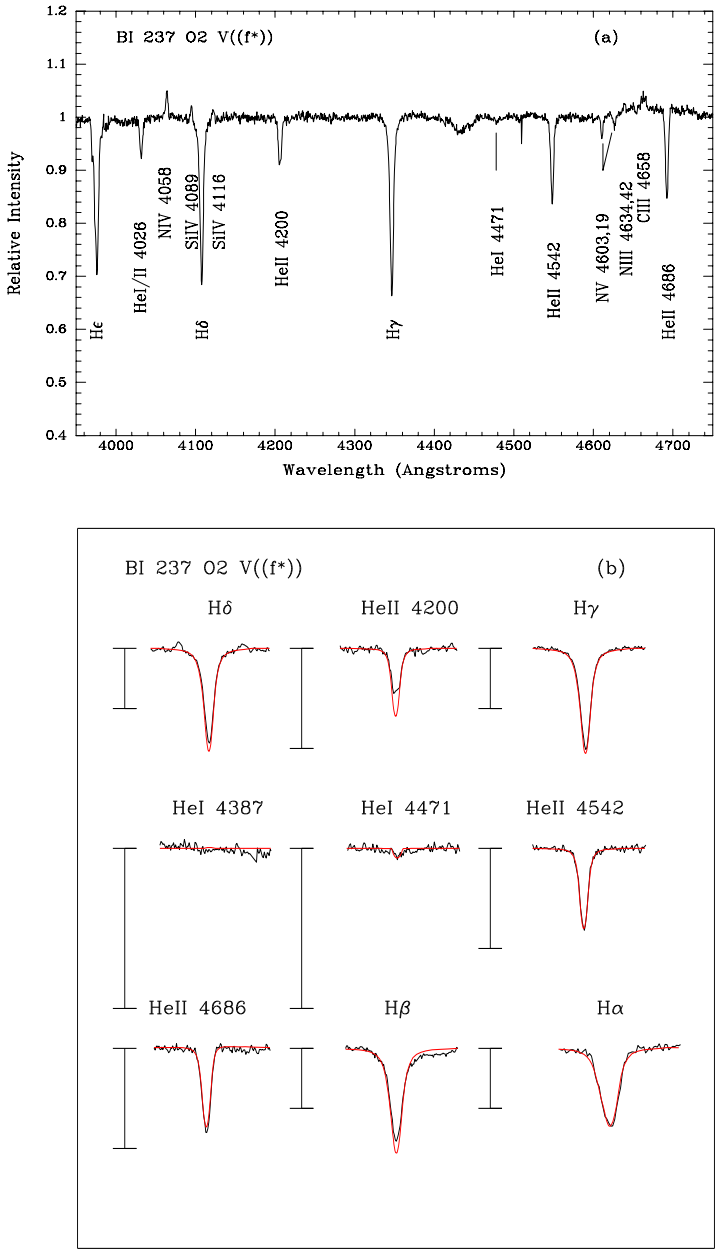

Fig. 12.— BI 237. Same as Fig. 1. A radial velocity of 430 km s^{-1} and a rotational broadening $v \sin i$ of 150 km s^{-1} was used in making this comparison. The He II λ4200 profile was is flat-bottomed, presumably due to a reduction problem, and not used in making the fit.

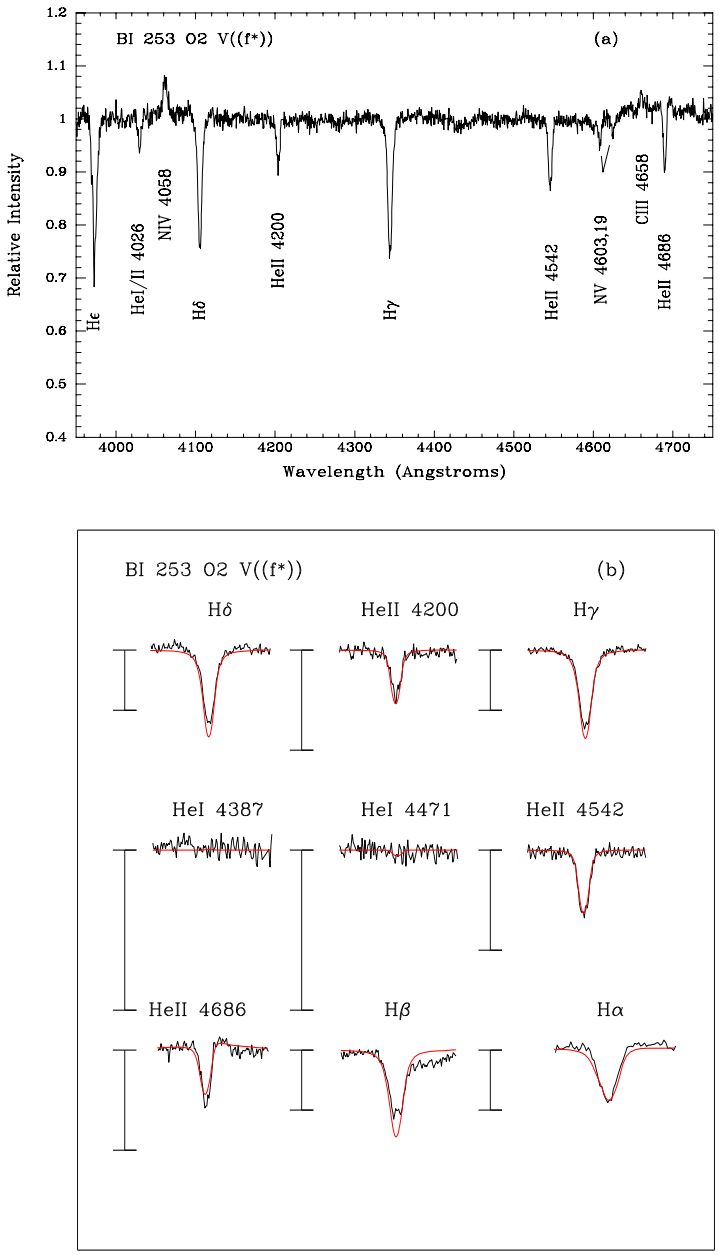

Fig. 13.— BI 253. Same as Fig. 1. A radial velocity of 270 km s^{-1} and a rotational broadening $v \sin i$ of 200 km s^{-1} was used in making this comparison.

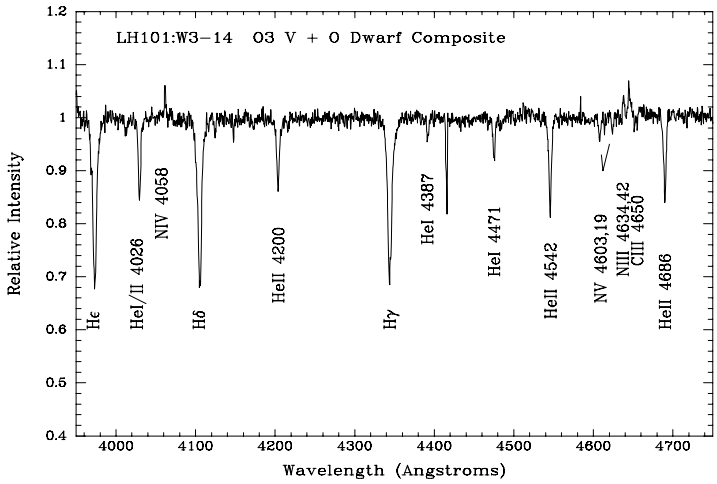

Fig. 14.— LH101:W3-14. The spectrum shown here is composite, with an O3 star dominating the nitrogen and He II spectra, and a later-type O star contributing the He I. No single model was able to fit the strengths of the He I and He II lines.

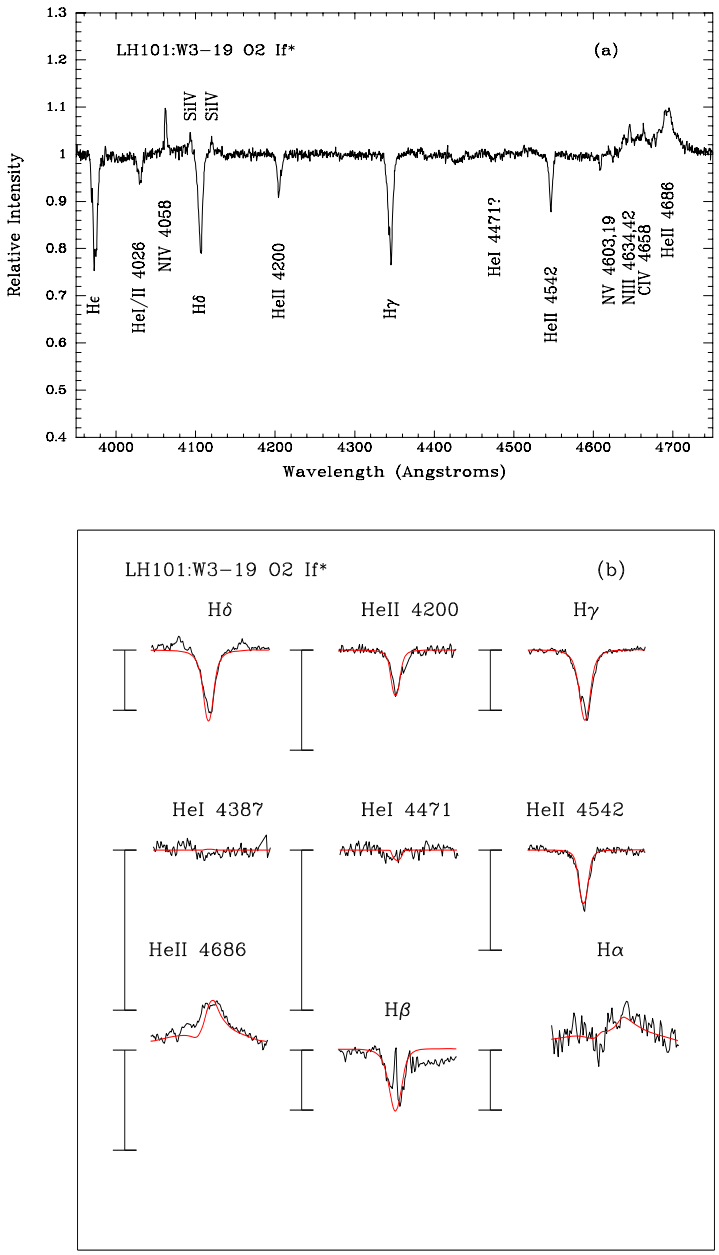

Fig. 15.— LH101:W3-19. Same as Fig. 1. A radial velocity of 320 km s^{-1} and a rotational broadening $v \sin i$ of 180 km s^{-1} was used in making this comparison.

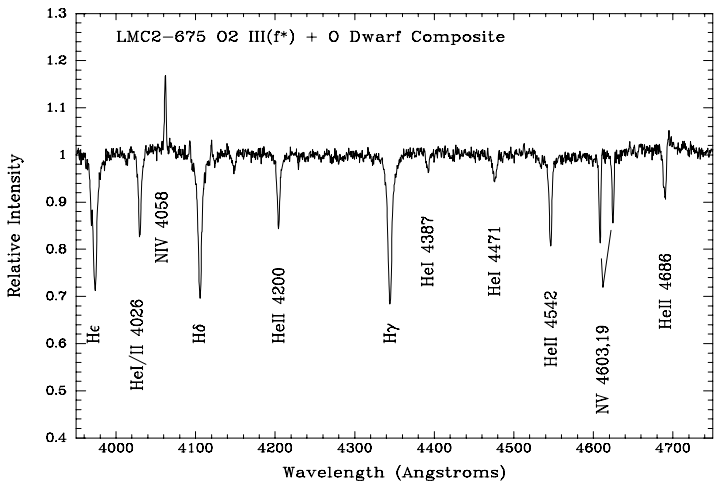

Fig. 16.— LMC2-675. The spectrum shown here is composite, with an O3 star dominating the nitrogen and He II spectra, and a later O-type star contributing the He I. As in Fig. 14, no single model was able to fit the strengths of the He I and He II lines.

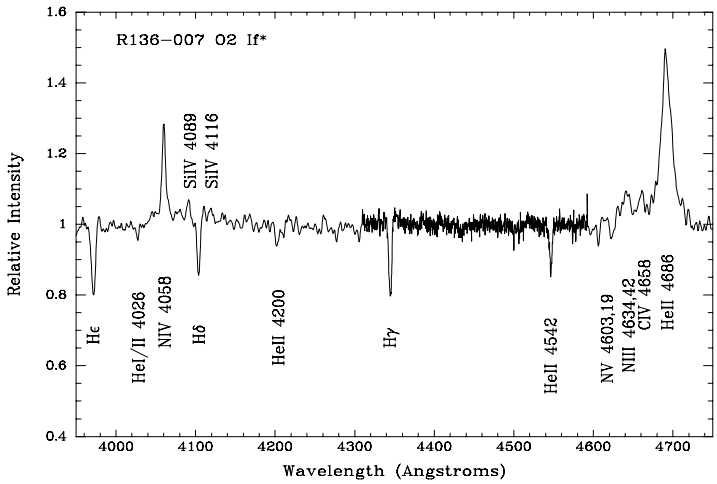

Fig. 17.— R136-007. We identify the major lines in the spectrum of R136-007. The data are from the FOS observations of Massey & Hunter (1998), except for the region 4310Å to 4590Å, where we have spliced in our higher S/N STIS spectrum. No combination of parameters led to a good fit, and we conclude that the star is composite, consistent with the discovery of eclipses in the light-curve by Massey et al. (2002).

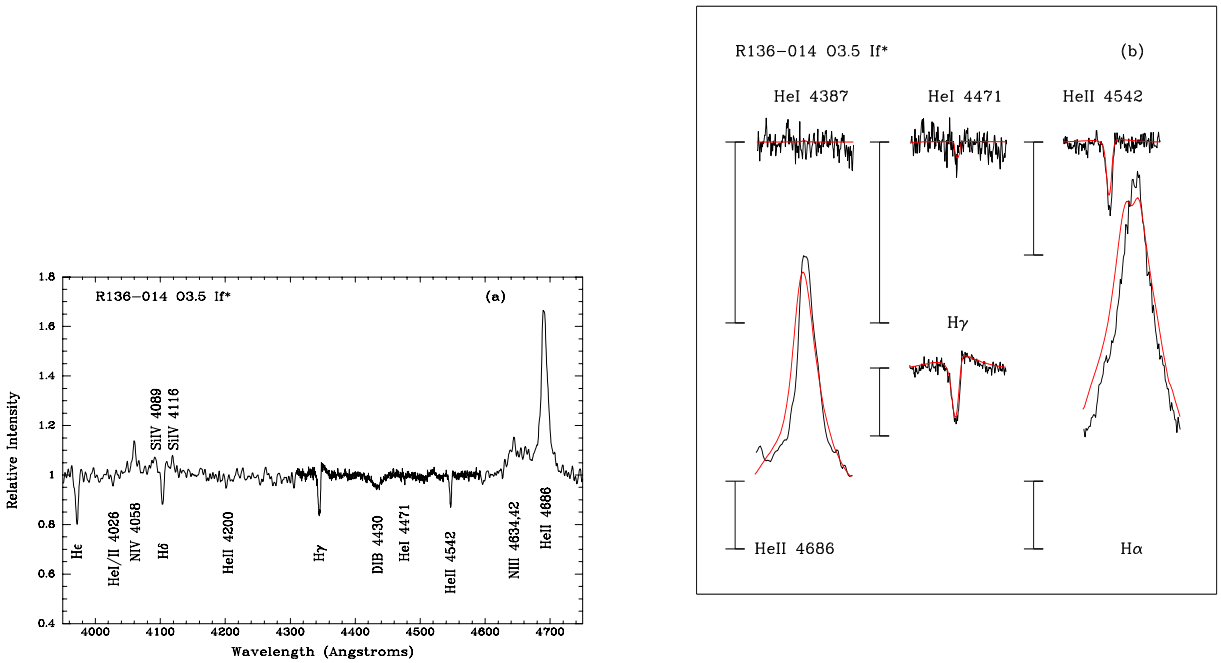

Fig. 18.— R136-014. The data in (a) come from the FOS observations of Massey & Hunter (1998), except for the region 4310Å to 4590Å, where we have spliced in our higher S/N STIS spectrum. In (b) the profiles are from the STIS data, except for that of He II λ4686, which comes from the FOS data. The colors and symbols have the same meaning as in Fig. 1. Problems with the STIS wavelength zero-point preclude determining an accurate radial velocity; a rotational broadening $v \sin i$ of 120 km s^{-1} was used in making this comparison.

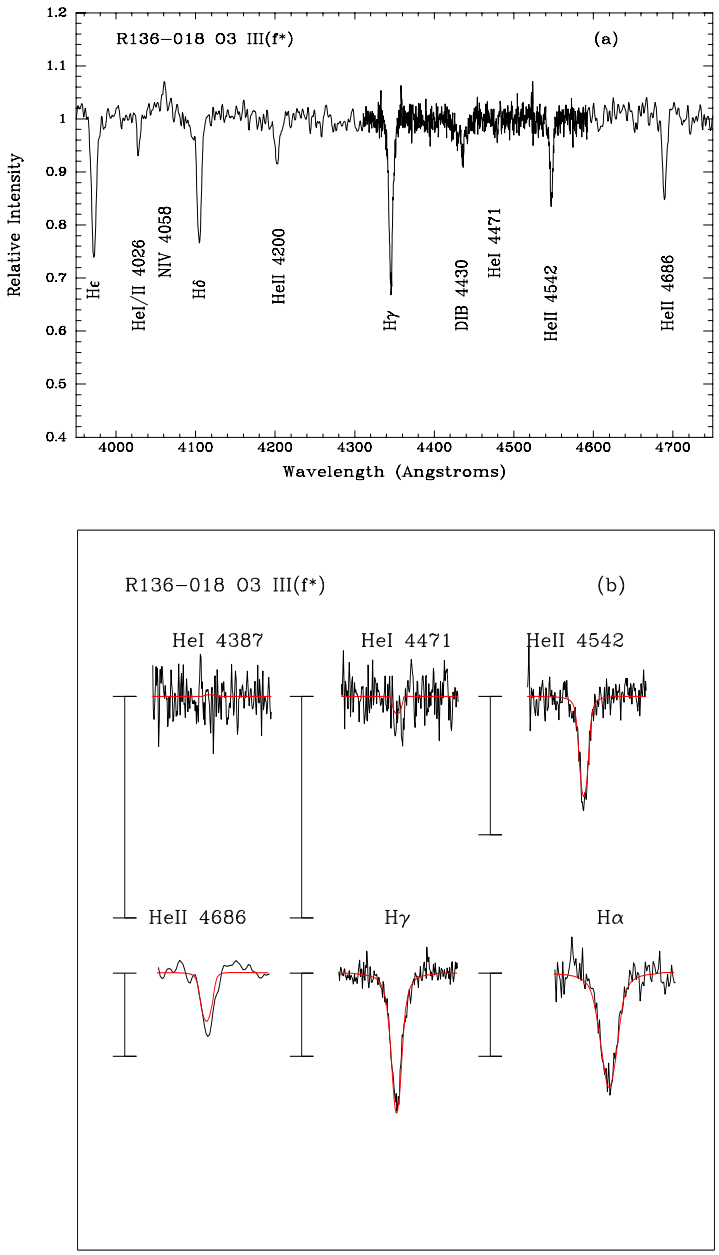

Fig. 19.— R136-018. Same as Fig. 18. A rotational broadening $v \sin i$ of 180 km s^{-1} was used in making this comparison.

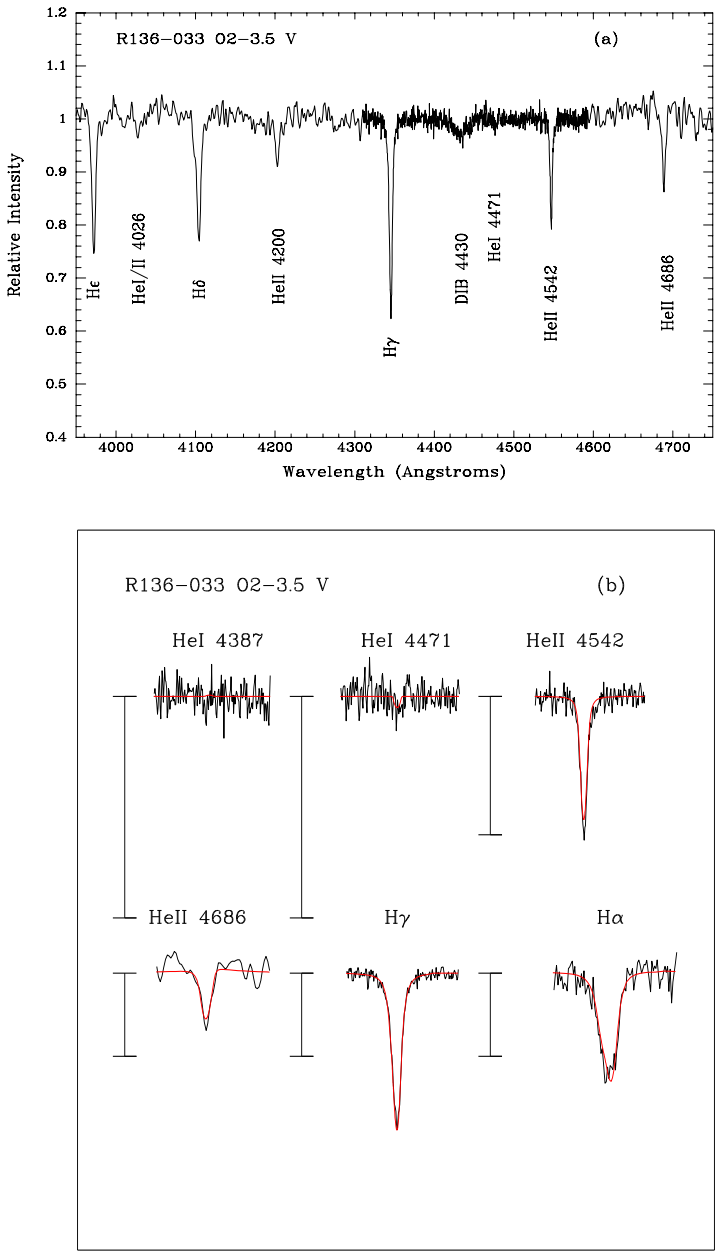

Fig. 20.— R136-033. Same as Fig. 18. A rotational broadening $v \sin i$ of 120 km s^{-1} was used in making this comparison.

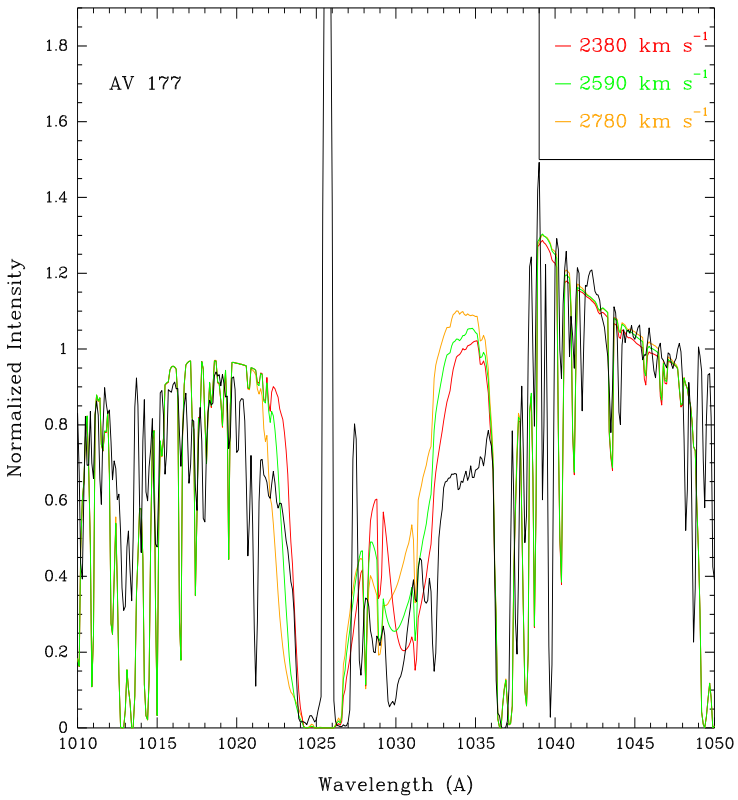

Fig. 21.— The O VI $\lambda\lambda 1032, 38$ doublet in AV 177. The black line shows the observed *FUSE* spectrum, while the color curves are the WM-BASIC models computed with terminal velocities v_∞ =2380 (red), 2590 (green), and 2380 (yellow) km s^{-1}. The best value determined from the OVI line is thus about 2400 km s^{-1}, which can be compared to the value 2650 km s^{-1} adopted from the CIV and NV lines (Table 4. The model spectra have been adjusted for the radial velocity of the star.

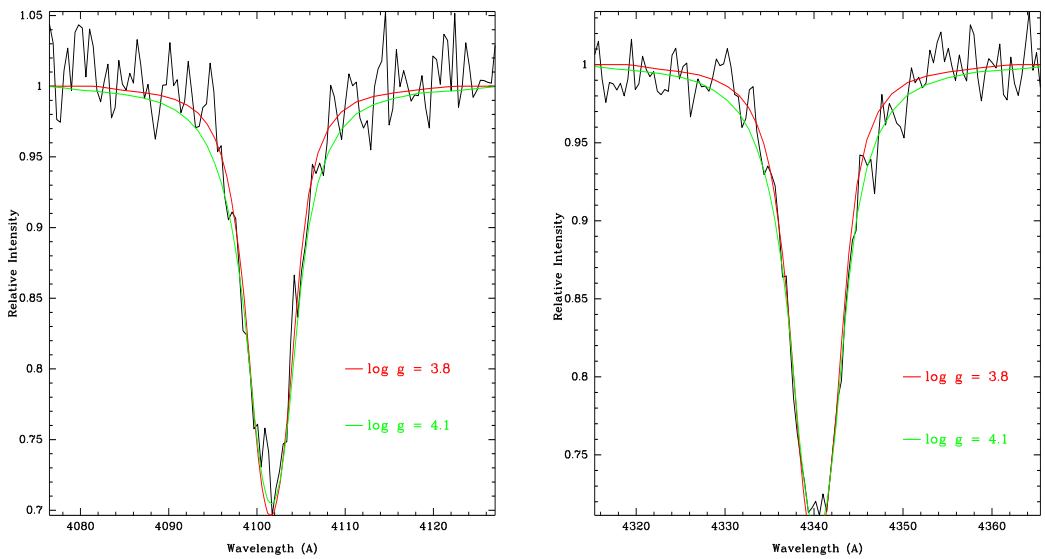

Fig. 22.— The effect that $\log g$ has on the Hδ and Hγ line profiles for AV 177. We show the model spectra for $\log g = 3.8$ (red) and 4.1 (green). The former gives a superior fit, although the higher surface gravity is indicated by the terminal velocity of the star if standard values are assumed for the force multiplier parameters.

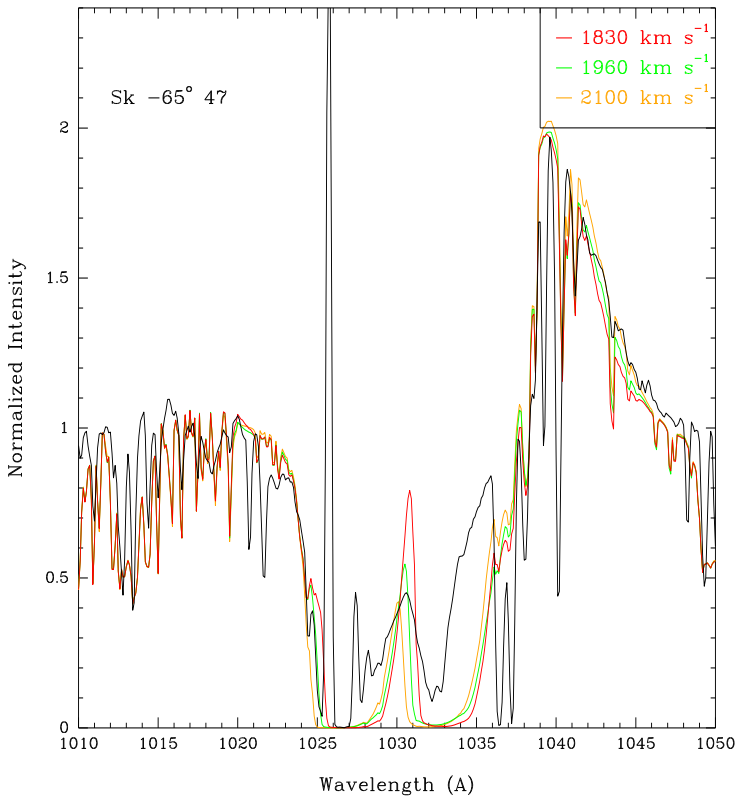

Fig. 23.— The O VI $\lambda\lambda 1032, 38$ doublet in Sk $-65°$ 47. The black line shows the observed *FUSE* spectrum, while the color curves are the WM-BASIC models computed with terminal velocities v_∞ =1830 (red), 1960 (green), and 2100 (yellow) km s^{-1}. The best value determined from the OVI line is thus about 2000 km s^{-1}, which can be compared to the value 2100 km s^{-1} adopted from the C IV line (Table 4. The model spectra have been adjusted for the radial velocity of the star.

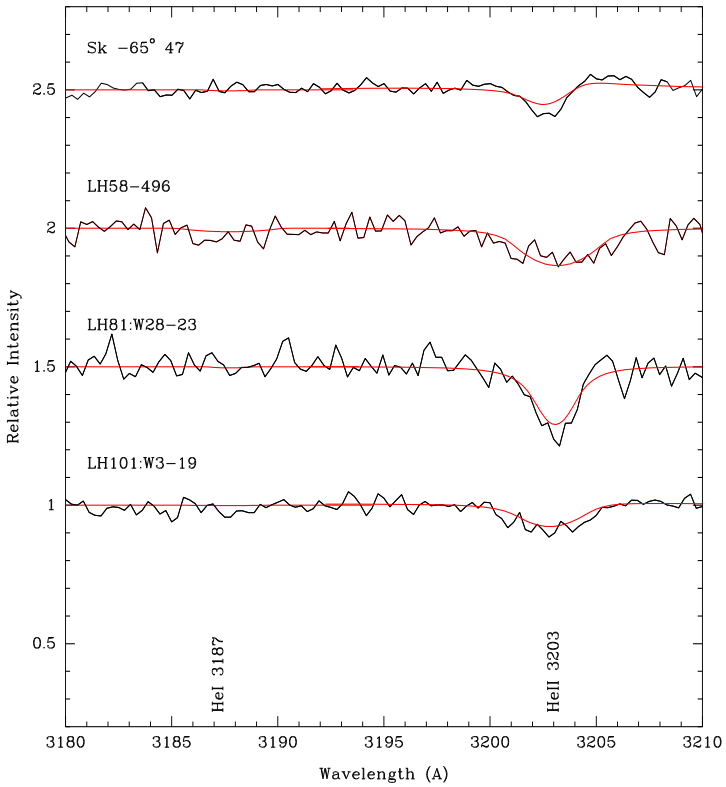

Fig. 24.— The FUV region. The region containing the He I λ3187 and He II λ3203 lines are shown for the four non-composite stars in our sample for which we have data in this region. Although we did not use this region in obtaining the final parameters, each star shows good agreement with the corresponding model.

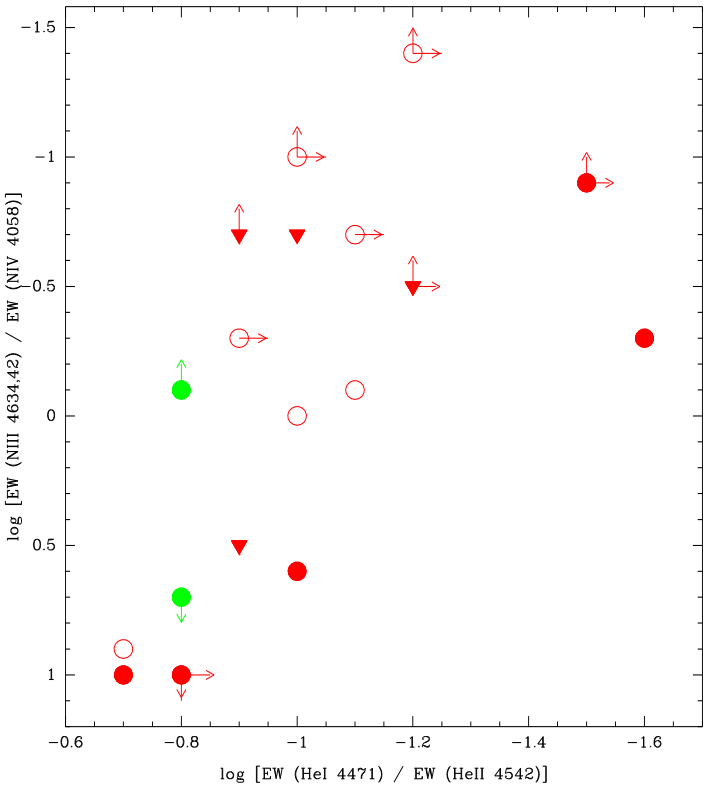

Fig. 25.— NIII/NIV vs HeI/HeII for O2-3.5 stars. The log of the ratio of the equivalent widths (EWs) of N III $\lambda 4634, 42$ to N IV $\lambda 4058$ emission is shown as a function of the log of the ratio of the EWs of He I $\lambda 4471$ to He II $\lambda 4542$. Dwarfs are shown as filled circles, giants are shown as filled triangles, and supergiants are shown as open circles. Red symbols are for the LMC stars; green for the SMC.

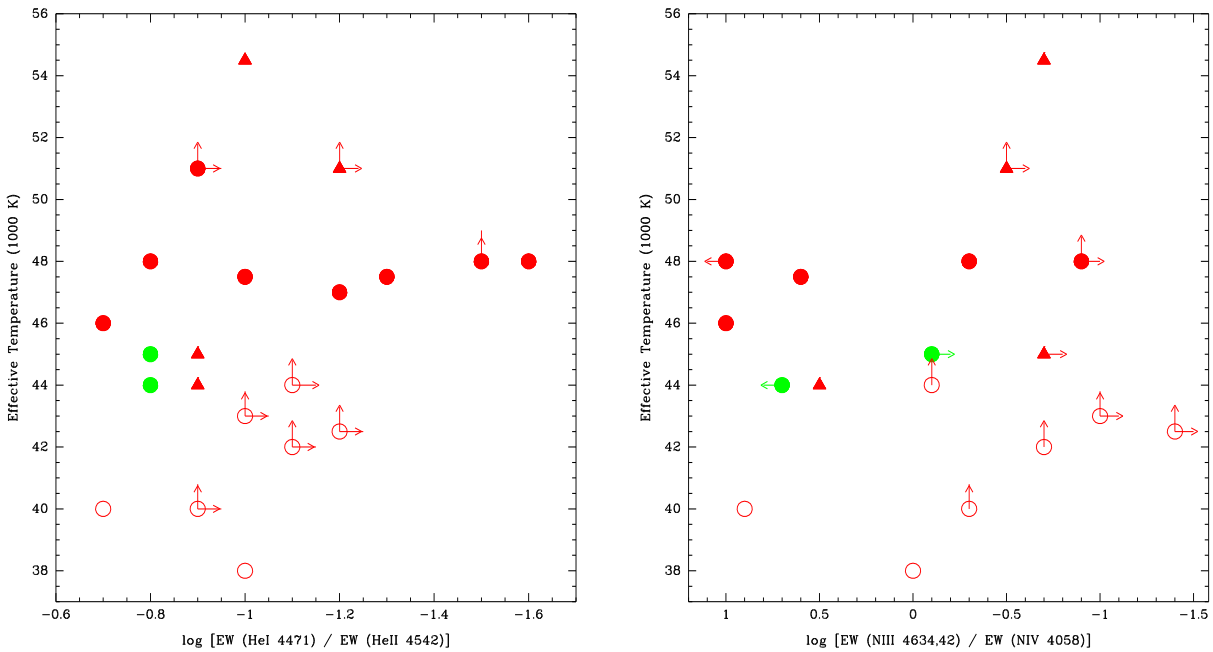

Fig. 26.— Effective temperatures of the earliest-type O stars (O2-O3.5) is shown as a function of (a) the HeI/HeII line ratio, and (b) the NIII/NIV emission line ratio. The symbols have the same meaning as in Fig. 25.

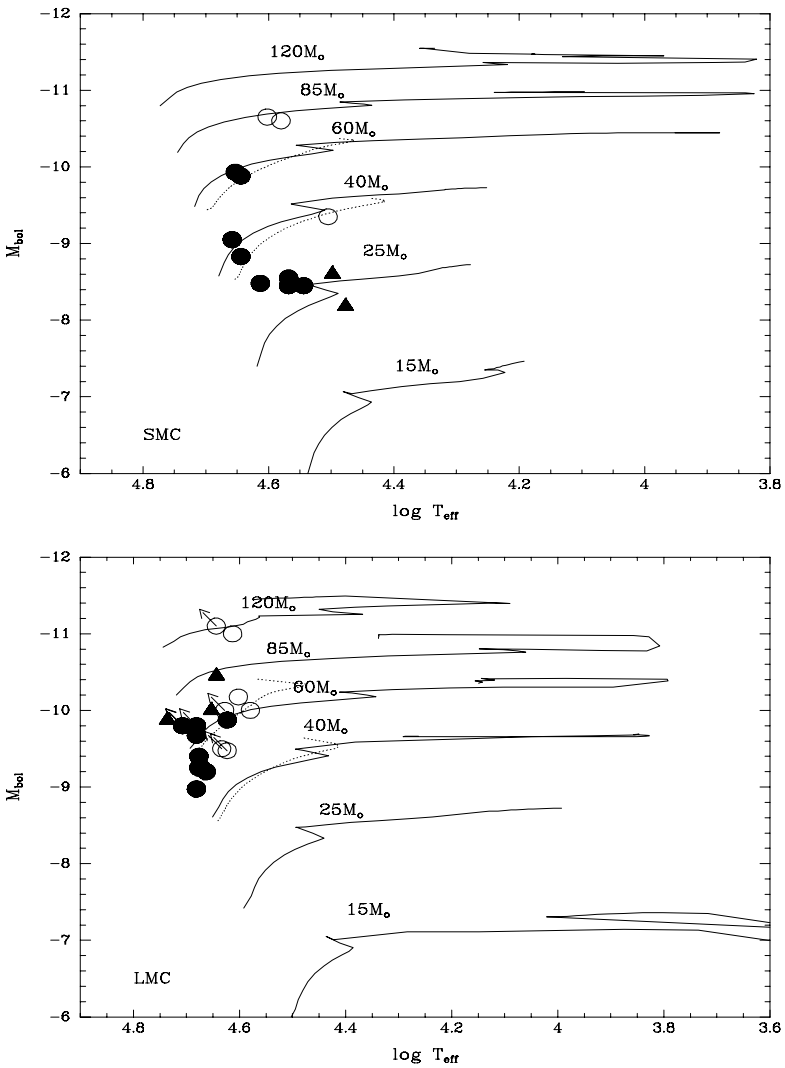

Fig. 27.— The location of our stars in the H-R diagram. Dwarfs are indicated by filled circles, giants by triangles, and supergiants by open circles. The non-rotating stellar evolutionary models of Charbonnel et al. (1993) are shown for the SMC, and those of Schaerer et al. (1993) are shown for the LMC. Only the H-burning part of the tracks are shown. For comparison, we include the newer rotation models (dotted lines) for initial masses of $60M_\odot$ and $40M_\odot$.

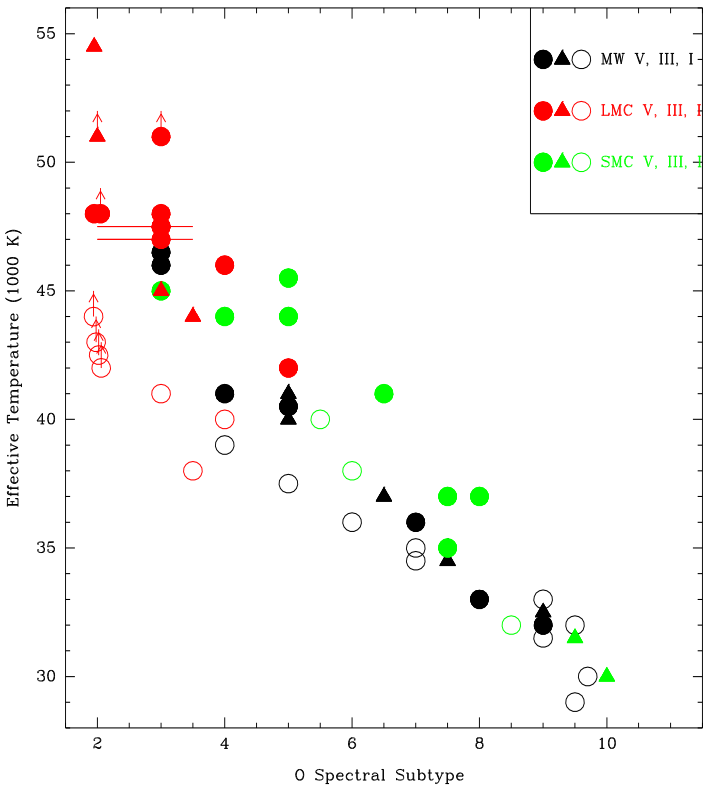

Fig. 28.— The effective temperatures as a function of spectral subtype, with a value of 2 denoting spectral type O2, 5.5 denoting O5.5, and "10" denoting B0. The filled circles for dwarfs; the filled triangles are giants, and the open circles are supergiants. Black symbols correspond to the Milky Way, red to the LMC, and green to the SMC. The data for the Milky Way is taken from Repolust et al. (2004); the data for the SMC and LMC are taken from Paper I and the present study.

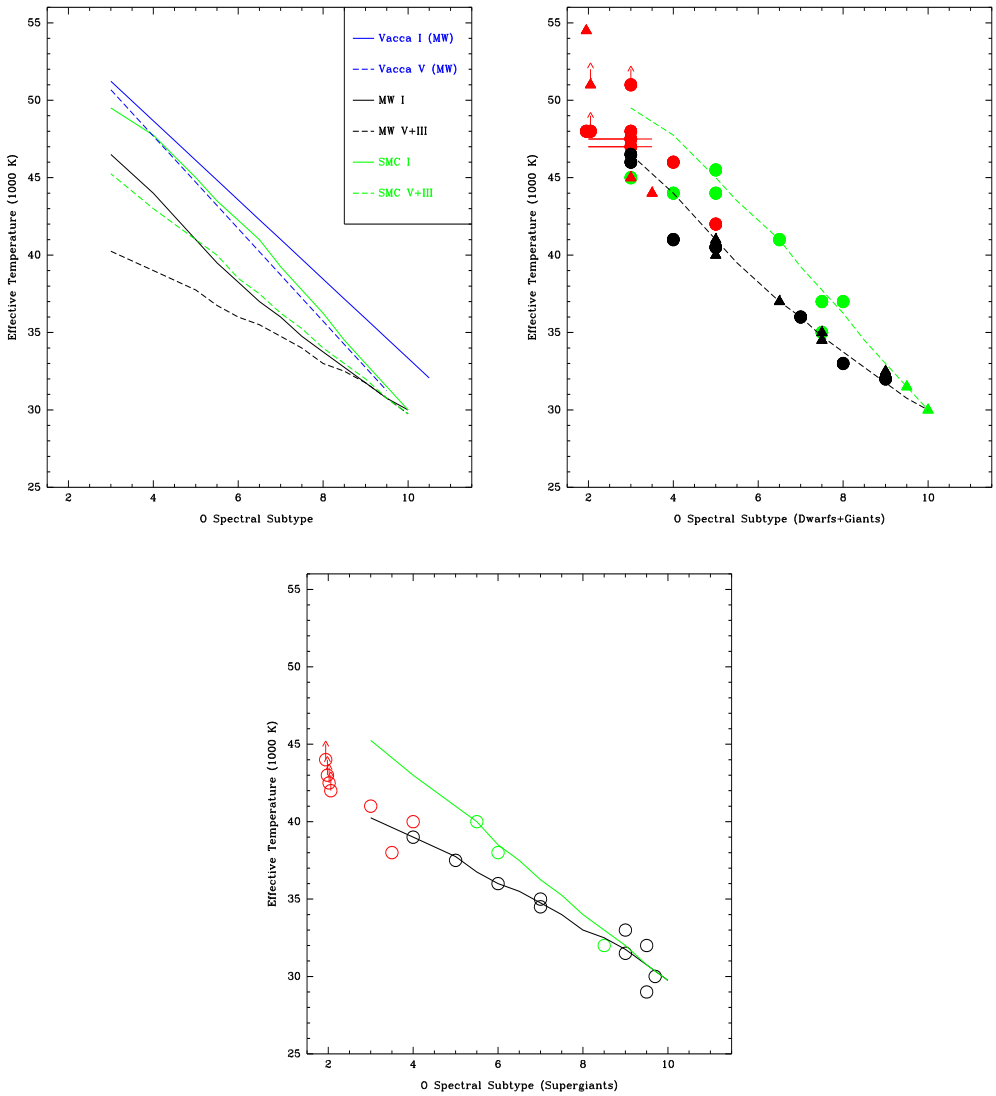

Fig. 29.— The effective temperature scale adopted here for the SMC (green) and the Milky Way (black). Solid lines denote the scale for supergiants; dashed lines are for dwarfs and giants. (a) The supergiant and dwarf effective temperature scales from Vacca et al. (1996) are shown for comparison in blue. (b) The effective temperature scale is shown with comparison for the data for the dwarfs and giants. (c) The supergiant effective temperature scale is shown in comparison with the data. The LMC scale is assumed to be intermediate between that of the SMC and the Milky Way.

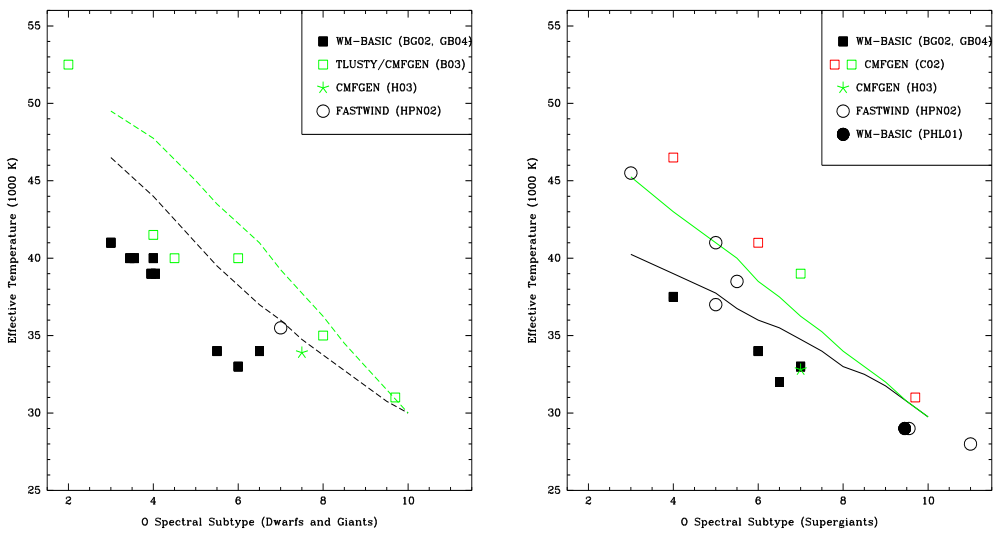

Fig. 30.— Our effective temperature scales (dashed or solid curves) are compared to recent data from others. Black symbols represent the Milky Way; red, the LMC; and green, the SMC. The different symbols are indicated in the key, where the data come from Bianchi & Garcia (2002), [BG02]; Garcia & Bianchi (2004), [GB04]; Crowther et al. (2002), [C02]; Hillier et al. (2003), [H03]; and Herrero et al. (2002), [CPN02], and Bouret et al. (2003).

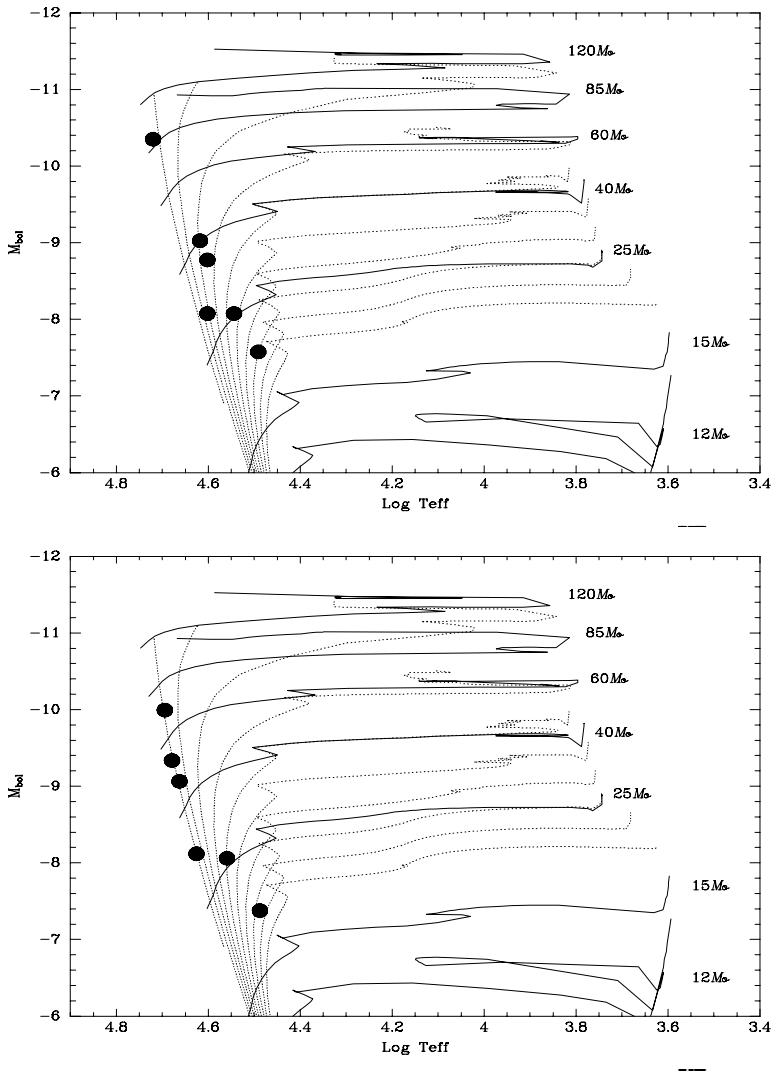

Fig. 31.— . The H-R diagram for the six stars studied by Bouret et al. (2003). The evolutionary tracks (solid lines) are from Charbonnel et al. (1993) computed for a metallicity of Z=0.04. The dotted lines are isochrones computed form these models for ages of 1-10 Myr at intervals of 1 Myr. (a) Stars placed with the parameters of Bouret et al. (2003). (b) Stars placed using the average spectral type to effective temperature calibration given here. In both cases the same photometry and color excesses were used, although a more realistic estimate of the reddening would result in stars about 0.1 mag more luminous.

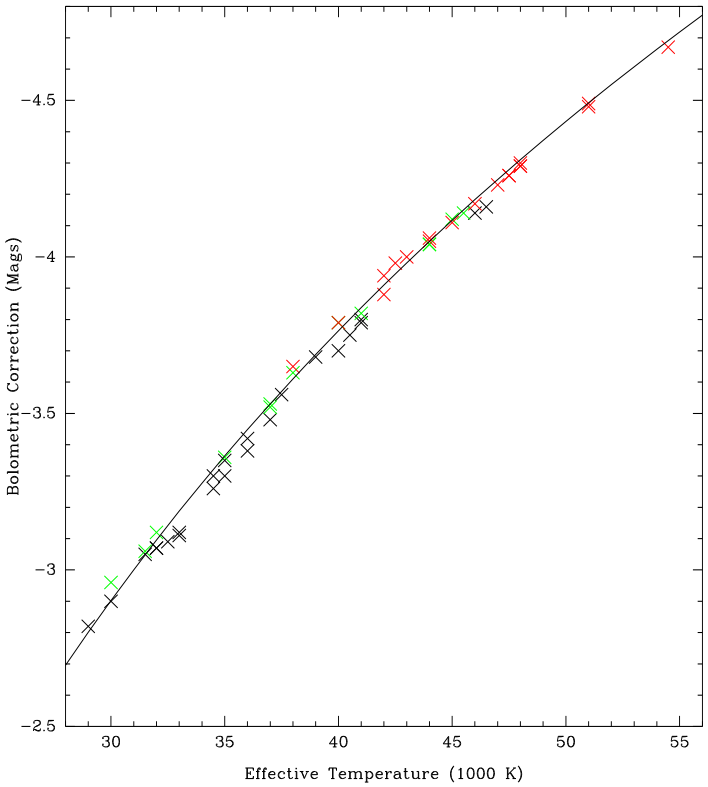

Fig. 32.— The bolometric corrections are shown as a function of effective temperature. The black points are for the Milky Way; the red points are for the LMC, and the green points are for the SMC. The smooth curve denotes the relationship given in Equ. 2.

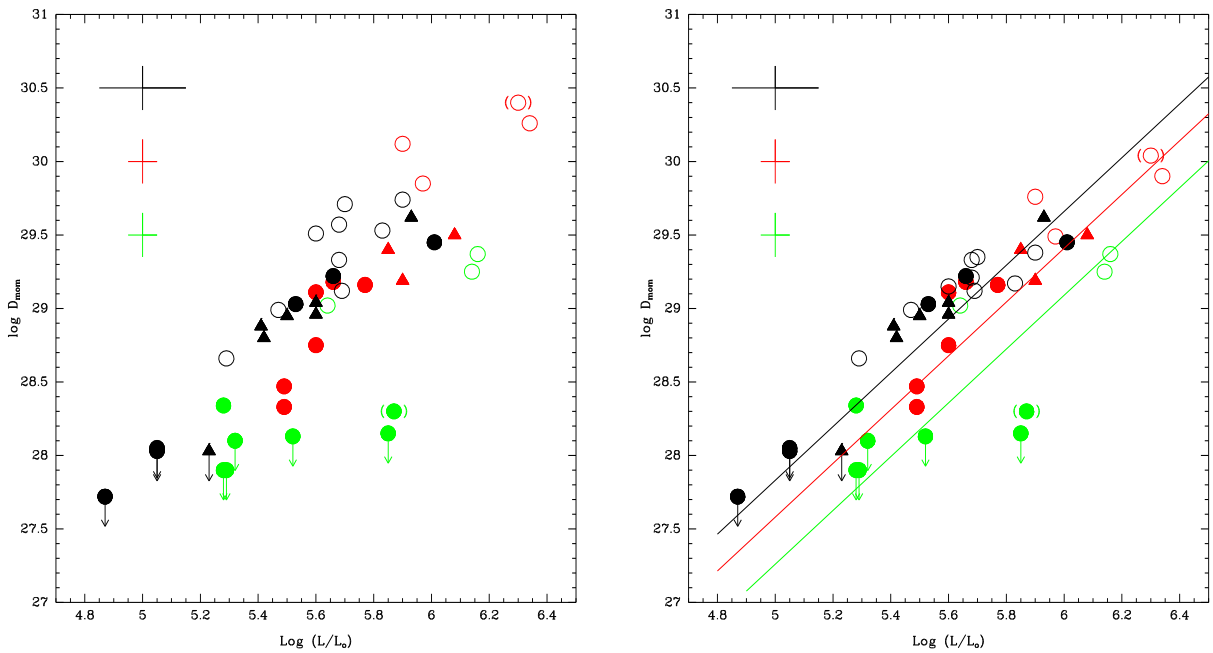

Fig. 33.— The modified wind momentum luminosity relationship. The symbols have the same meaning as in Fig. 28. Stars with only lower limits on their effective temperatures are not shown, and stars whose values are particularly uncertain are indicated by parenthesis. Typical error bars are shown in the upper left. (a) The data are shown uncorrected for wind clumping. (b) The stars showing Hα emission have been corrected by -0.36 dex in $D_{\rm mom}$ to correct for the effects of wind clumping on the deduced mass-loss rates. The three lines are *not* fits to the data; instead, these are the theoretical expectations from radiatively driven wind theory.

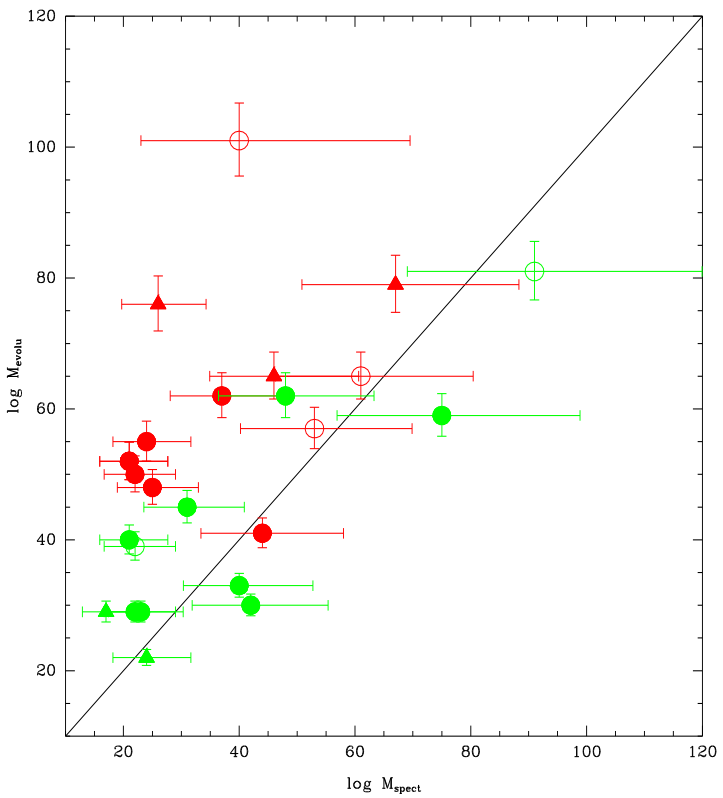

Fig. 34.— The evolutionary masses are compared to the spectroscopic masses. The symbols have the same meaning as in Fig. 28.